

A PRELIMINARY DESIGN METHOD FOR AXIAL FLOW COMPRESSOR STAGES



by
Metin Mehel

Submitted to Graduate School of Natural and Applied Sciences
in Partial Fulfillment of the Requirements
for the Degree of Master of Science in
Mechanical Engineering

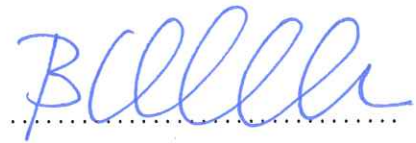
Yeditepe University

2019

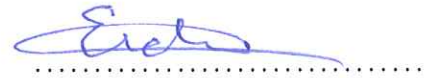
A PRELIMINARY DESIGN METHOD FOR AXIAL FLOW COMPRESSOR STAGES

APPROVED BY:

Assoc. Prof. Dr. Ali Bahadır Olcay
(Thesis Supervisor)
(Yeditepe University)



Prof. Dr. Erdem An
(Yeditepe University)



Assoc. Prof. Dr. Emre Alpman
(Marmara University)



DATE OF APPROVAL: / / 2019

ACKNOWLEDGMENTS

It is with immense gratitude that I acknowledge the support and help of my advisors assoc. Prof. Dr. A. Bahadır OLCAY and Emre ALPMAN. Pursuing my thesis under their supervision has been an experience that broadens the mind and presents an unlimited source of learning.

Finally, I would like to thank my wife Dilek Ceref MEHEL, my two sons Yusuf and Ali, and my brother Yavuz Selim MEHEL for their endless love, patient and support.

ABSTRACT

A PRELIMINARY DESIGN METHOD FOR AXIAL FLOW COMPRESSOR STAGES

A preliminary design method for axial flow compressor stages and mean line code were developed based on steady-state energy equations and empirical correlations.

Axial flow compressors typically have three common annulus shapes, which are called as the constant hub, constant tip, and constant mean diameter. Each type of design has its own specific advantages and disadvantages compared to others. Due to customer requirements, such as disk stress, space for accessories, overall length, etc. Designers sometimes need to utilize variable mean diameter annulus shape, which has no constant diameter and provides a more flexible design.

In this thesis, variable mean diameter compressor calculations were done through the mean line radius then corresponding blade angles were determined by using empirical correlations. Tip and hub air angles were determined by utilizing the radial equilibrium equation. The tool is called “Axial Compressor Mean Line Calculation” (ACMC), which is a spreadsheet-based Excel VBA tool. In order to get maximum efficiency and compression ratio, an optimum combination of flow path dimensions and air angles was found by the optimization process. Design of experiment (DOE), response surface and multi-objective genetic algorithm optimization were conducted with Ansys Workbench. The first stage of an axial compressor was designed with the code and 3D CFD results were compared with ACMC results. Mass flow rate variation was 2.4600 percent, compression ratio variation was 0.1864 percent and efficiency variation was 2.1597 percent between CFD and analytical solution.

ÖZET

EKSENEL AKIŞLI KOMPRESÖR KADEMELERİ İÇİN BİR ÖN TASARIM METODU

Eksenel akışlı kompresör kademeleri için bir ön tasarım metodu ve orta hat hesaplama kodu denge durumu enerji denklemleri ve test korelasyonları kullanılarak geliştirildi.

Kompresör tasarımında genel olarak 3 tip akış yolu bulunmaktadır. Bunlar, sabit kök, sabit dış ve sabit orta hat çaplı akış yolları olarak adlandırılırlar. Her bir akış yolu tipi kendine has avantajlar ve dezavantajlar barındırmaktadır. Diğer taraftan müşteri kısıtlamaları, örneğin disk gerilmeleri, ekipmanlar için boş alan, toplam boy v.b. nedeniyle tasarımcılar sabit çap barındırmayan değişken orta hatlı akış yolu tipini kullanmaktadırlar. Böylece daha serbest tasarım imkanı sağlanmaktadır.

Bu tezde, değişken orta hatlı kompresör hesaplamaları orta hat yarı çapında yapıldı ve ilgili kanat açıları deneysel korelasyonlarla bulundu. Dış ve kök çaplarındaki akışkan açıları radyal denge formüllerinden faydalanılarak hesaplandı. Geliştirilen kod, APMC olarak adlandırılmış olup Excel ve “Visual Basic for Applications” (VBA) temelli bir tasarım aracıdır. Maksimum verim ve basma oranını bulabilmek için optimizasyon süreciyle akış yolu ölçülerinin ve akış açılarının en uygun kombinasyonu bulundu. Deney tasarımı, cevap yüzeyi ve çoklu hedefli genetik algoritma optimizasyonu Ansys Workbench üzerinden yapıldı. Eksenel kompresörün ilk kademesi tasarlanmış olup hesaplamalı akışkanlar dinamiği sonuçlarıyla 1 boyutlu orta hat hesaplamaları karşılaştırıldı; kütleli debide yüzde 2.4600, basma oranında yüzde 0.1864 ve verimde yüzde 2.1597 farklar gözlemlendi.

TABLE OF CONTENTS

| | |
|--|------|
| ACKNOWLEDGMENTS | iii |
| ABSTRACT..... | iv |
| ÖZET | v |
| LIST OF FIGURES | viii |
| LIST OF TABLES..... | xi |
| LIST OF SYMBOLS/ABBREVIATIONS..... | xii |
| 1. INTRODUCTION..... | 1 |
| 2. AXIAL COMPRESSOR BASICS | 4 |
| 3. AXIAL COMPRESSORS MEAN LINE DESIGN | 9 |
| 3.1. DEFINITION OF MEAN LINE DESIGN | 9 |
| 3.2. AERODYNAMIC DESIGN OF AXIAL COMPRESSOR..... | 9 |
| 3.2.1. Thermodynamic Calculations in an Axial Compressor Stage..... | 9 |
| 3.2.2. The Factors Which Affect Pressure Ratio | 13 |
| 3.2.3. Radial Equilibrium in a Fluid Element..... | 14 |
| 3.2.4. Annulus Types of Axial Compressor..... | 17 |
| 3.2.5. Blockage and Work Done Factor..... | 19 |
| 3.2.6. Degree of Reaction | 20 |
| 3.2.7. Pitch to Chord Ratio, Hub to Tip Ratio, and Aspect Ratio..... | 22 |
| 3.2.8. Diffusion Factor (DF) and De Haller (DH) Criterion..... | 23 |
| 3.2.9. Cascade Notation, Incidence and Deviation Calculations | 26 |
| 3.2.10. Work and Flow Coefficient..... | 31 |
| 3.2.11. Losses and Efficiency in Axial Compressors..... | 31 |
| 3.2.12. Initial Sizing and Shaft Speed Calculations for a Stage..... | 38 |
| 3.3. PRELIMINARY MECHANICAL DESIGN OF AXIAL COMPRESSOR | 39 |
| 3.3.1. Centrifugal Stress at Blade Root Section..... | 39 |
| 3.3.2. Blade Resonance..... | 40 |
| 3.4. OPTIMIZATION PROCESS..... | 41 |
| 3.4.1. Design of Experiment | 41 |
| 3.4.2. Polynomial Response Surface Method..... | 43 |

3.4.3. Multi Objective Genetic Algorithm Optimization.....44

4. ACMC TOOL CALCULATION PROCEDURE46

4.1. FORMULATIONS47

5. COMPARING ACMC TOOL AND CFD RESULTS.....53

6. CONCLUSION71

REFERENCES72



LIST OF FIGURES

| | |
|--|----|
| Figure 2.1. Schematic view of Brayton cycle..... | 4 |
| Figure 2.2. General view of an axial compressor. | 5 |
| Figure 2.3. A general view for rotor and stator embodiment in a compressor stage..... | 8 |
| Figure 3.1. T-s and velocity diagram of a stage..... | 10 |
| Figure 3.2. Control volume through rotor passage | 11 |
| Figure 3.3. Force balance on a fluid element in a flow passage | 15 |
| Figure 3.4. Annulus types | 18 |
| Figure 3.5. Variation in the axial velocity of the fluid along the span | 19 |
| Figure 3.6. Mean work done factor with respect to the number of stages..... | 20 |
| Figure 3.7. Variation of frictional losses with respect to diffusion factor | 24 |
| Figure 3.8. Correlation of wake momentum thickness with an equivalent diffusion factor at a minimum loss incidence angle | 25 |
| Figure 3.9. Relative velocity distribution over suction and pressure surfaces of blade | 26 |
| Figure 3.10. Simple cascade test setup | 27 |
| Figure 3.11. Cascade test aerofoil notation..... | 28 |
| Figure 3.12. Variation of stagnation pressure loss and deflection for cascade at a certain incidence | 29 |
| Figure 3.13. Mean deflection and mean stagnation pressure loss for a cascade of the fixed geometrical form..... | 30 |
| Figure 3.14. Forces acting on the cascade | 32 |

| | |
|---|----|
| Figure 3.15. Lift & profile drag coefficients for a cascade of the fixed geometrical form | 33 |
| Figure 3.16. Basic wave types | 35 |
| Figure 3.17. Shock loss model of Miller et al. | 36 |
| Figure 3.18. Face centred CCD design space | 42 |
| Figure 4.1. Block diagram for ACMC design procedure | 47 |
| Figure 4.2. ACMC tool layout | 48 |
| Figure 5.1. Stage calculations at ACMC of initial design point, Part-1 | 54 |
| Figure 5.2. Stage calculations at ACMC of initial design point, Part-2 | 55 |
| Figure 5.3. Stage calculations at ACMC of initial design point, Part-3 | 56 |
| Figure 5.4. Stage calculations at ACMC of initial design point, Part-4 | 57 |
| Figure 5.5. Post-processing parameters of ACMC of initial design point | 58 |
| Figure 5.6. The variation between parameters of initial and optimum design points | 61 |
| Figure 5.7. FEA model of the blade with root attachment | 62 |
| Figure 5.8. Parametric NX blade model | 62 |
| Figure 5.9. Von Misses Stress plot of the blade | 63 |
| Figure 5.10. Grid structure for rotor and stator passages | 65 |
| Figure 5.11. Y+ plot at surfaces | 65 |
| Figure 5.12. Meridional view of blockage region between Station-3 and Station-4 | 66 |
| Figure 5.13. Closer view to blockage region between Station-3 and Station-4 | 67 |
| Figure 5.14. Blade to blade view, Relative Mach Number plot at 90% span | 68 |
| Figure 5.15. Isentropic Mach Number plot around blade at 90% span | 68 |

| | |
|--|----|
| Figure 5.16. Blade to blade view, Relative Mach Number plot at 50% span..... | 69 |
| Figure 5.17. Isentropic Mach Number plot around blade at 50% span | 69 |
| Figure 5.18. Blade to blade view, Relative Mach Number plot at 10% span..... | 70 |



LIST OF TABLES

| | |
|--|----|
| Table 3.1. The number of experiment in the Face Centred CCD method | 43 |
| Table 5.1. Performance parameters of initial design point | 59 |
| Table 5.2. Input parameters, upper and lower limits for optimization | 59 |
| Table 5.3. Comparing input and output parameters before and after optimization | 60 |
| Table 5.4. The variation between CFD and analytical solution..... | 66 |

LIST OF SYMBOLS/ABBREVIATIONS

| | |
|---------------|--|
| a | Maximum camber distance from leading-edge |
| c | Cord length or local acoustic velocity |
| c_p | Specific heat at constant pressure |
| C | Absolute velocity |
| C_a | Axial velocity |
| C_D | Overall drag factor |
| C_{DA} | End wall drag coefficient |
| C_{Dp} | Profile drag coefficient |
| C_{DS} | Secondary losses drag coefficient |
| C_L | Lift coefficient |
| C_w | Tangential air velocity (Whirl) |
| C_{w1} | Tangential air velocity at blade inlet |
| C_{w2} | Tangential air velocity at blade outlet |
| $C_{w2,root}$ | Tangential air velocity at blade outlet at the hub |
| $C_{w2,mean}$ | Tangential air velocity at blade outlet at mean line |
| $C_{w2,tip}$ | Tangential air velocity at blade outlet at the tip |
| C_1 | Absolute velocity at rotor inlet |
| C_2 | Absolute velocity at rotor outlet |
| C_3 | Absolute velocity at stator inlet |
| C_4 | Absolute velocity at stator outlet |
| DF | Difusion factor |
| DF_{eq} | Equivalent difusion factor |
| DH | De Haller Number |
| F | Centrifugal force applied on fluid element |
| \vec{F} | Pseudo objective function |
| h_0 | Stagnation enthalpy |
| h | Static enthalpy |
| i | Incidence angle |
| Mach | Mach number |

| | |
|---------------|------------------------------------|
| NB | Number of blades |
| N | Shaft speed |
| n_b | Blade efficiency |
| n_s | Stage efficiency |
| p_0 | Total pressure |
| p | Static pressure |
| P | Power |
| r | Radius |
| s | Pitch |
| T_0 | Stagnation temperature |
| T | Static temperature |
| U | Tangential speed of blade |
| V | Air velocity in cascade |
| W | Relative velocity of flow |
| \bar{w} | Mean loss |
| w | Total loss factor |
| \vec{X} | Input vector |
| z_i | Weight factor |
| α_m | Vector mean angle |
| α_1 | Air inlet absolute velocity angle |
| α'_1 | Stator aerofoil inlet angle |
| α_2 | Air outlet absolute velocity angle |
| α'_2 | Stator aerofoil outlet angle |
| β_1 | Blade relative air inlet angle |
| β'_1 | Blade aerofoil inlet angle |
| β_2 | Blade relative air outlet angle |
| β'_2 | Blade aerofoil outlet angle |
| Λ | Degree of reaction |
| δ | Deviation angle |
| ε | Deflection |
| γ | Heat capacity ratio |

| | |
|-----------------|--|
| λ | Work done factor |
| ξ | Stagger angle |
| ω | Angular velocity |
| ρ | Fluid density |
| σ_{root} | Centrifugal root stress |
| τ | Torque |
| θ | Blade camber angle |
| ψ | Work coefficient |
| ϕ | Flow coefficient |
| ACMC | Axial compressor mean line calculation |
| AR | Aspect ratio |
| CCD | Central composite design |
| CPR | Compression ratio |
| DH | De Haller number |
| DF | Diffusion factor |
| DOE | Design of experiment |
| FCCCD | Face centred central composite design |
| HTR | Hub to tip ratio |
| IGV | Inlet guide vane |
| MCA | Multiple circular arc |
| MOGA | Multi objective genetic algorithm |
| OGV | Outlet guide vane |
| PCR | Pitch to chord ratio |
| VBA | Visual Basic for applications |

1. INTRODUCTION

Aircraft, which are used in high speed and long-range applications, mostly have gas turbines engines as propulsion units. Axial type compressors are preferred due to their high efficiency, high-pressure ratio and high flowrate capability compared to the air inlet area.

The basic design objectives of the axial compressor are to provide high mass flow rate and pressure ratio, efficiency in terms of power, being small in longitudinal size and reasonable surge margin.

The aerodynamic design of the compressors typically starts with 1D mean line analysis based on steady-state energy equations and empirical correlations. This process is cheap in terms of computational memory and CPU time but it has low fidelity compared to 2D Through Flow analysis, 2D Blade to Blade analysis and 3D CFD analysis.

1D mean line analysis approach is still used by many design systems as an initial step because it can converge about 60-70 percent to the final design [1]. Relatively simple calculation steps allow designers to determine preliminary annulus shape, blade angles, and size, efficiency, performance maps, etc.

There are commonly three basic annulus shapes belong to axial compressors. They are classified based on the location where their constant diameter is assigned. Constant tip compressors have a constant diameter at tip or casing location. It is usually used in aircraft and missile engines. Mean diameter increases per stage numbers, eventually tangential speed increases. Temperature rise increases at later stages as well. Therefore less number of stages are required to obtain a given pressure ratio. Other advantages are less fluid deflection requirement and an increase in de Haller number [2]. On the other hand, relatively higher end-wall losses, higher disk stresses and small volume for externals (External equipment) are some of the disadvantages [3].

Constant hub compressors have a straight hub geometry. Therefore, disk manufacturing cost is less. Aerodynamic losses are less compared to constant tip design. Due to the decreasing outer diameter, more volume is available for externals. On the other hand, the descending mean radius results in lower tip speed at later stages. Therefore, higher loaded blades [4] and an increased number of stages is required with respect to constant tip and mean design. There

is more space for external equipment in this type of design because of decreasing outer diameter through later stages.

Constant mean diameter compressors have a straight mean diameter along the flow path. It provides easier calculation steps compared to the constant tip and hub design.

An additional annulus shape, which is called as, variable mean line, is a compromise among constant tip, hub and mean diameter annulus shapes. When customer requirements entail designers to limit or restrict some of the sizing parameters, variable mean line design, in conjunction with optimization methods is an option to find optimum design point in the given circumstances.

It is known that axial compressor mean line design is a sophisticated process because numerous output parameters should be kept in specific ranges by changing input parameters. Root, mean, hub diameters, air inlet, and outlet angles are the examples for input parameters; rotor and stator diffusion factors, compression ratio, mass flow rate and efficiency are the examples for output parameters. Changing input parameters manually in order to meet the performance criteria is not easy in case of looking for an optimum design point. It should be handled regarding a multi-objective optimization method.

An additional problem in axial compressor design is to fulfill customer requirements, such as geometric limitations, stress, weight and cost, manufacturability and assembly restrictions. The requirements may entail designers to build annulus shapes far from the aforementioned shapes (Constant tip, mean, hub) while maintaining performance criteria, such as aerodynamic efficiency, mass flow rate and compression ratio to admissible level. Designers sometimes need to make concessions between customer requirements and performance criteria. For instance, in order to maintain greater space for external equipment, tip diameters should be lowered which causes the compression ratio to diminish. The question is then, might it be possible to develop a mean line method in case of not having constant tip, hub and mean diameter due to customer requirements? Would the admissible efficiency and compression ratio still be attained?

Several studies were conducted about improving 1D mean line methods [5-7]; Falck [1] used constant mean diameter and relevant assumptions in their design methods, Miller [8] used the constant hub, mean and tip diameter in his design method. Those mentioned

methods could not offer any resolution that considers both customer requirements and performance criteria simultaneously.

In this thesis, it is emphasized to develop a method, which offers flexibility to designers to be able to set desired parameters to specified values then remained values are managed by optimization process to meet performance criteria utilizing DOE, response surface, multi-objective genetic algorithm optimization method.



2. AXIAL COMPRESSOR BASICS

Brayton cycle is the ideal cycle for gas turbine engines, which consists of a compressor, combustion chamber, and turbine modules. The process scheme is illustrated in Figure 2.1.

All gas turbines have a compressing unit which is called a compressor. Compressors are basically used so as to increase the pressure of the working fluid e.g. air and maintain the required mass flowrate for the combustor.

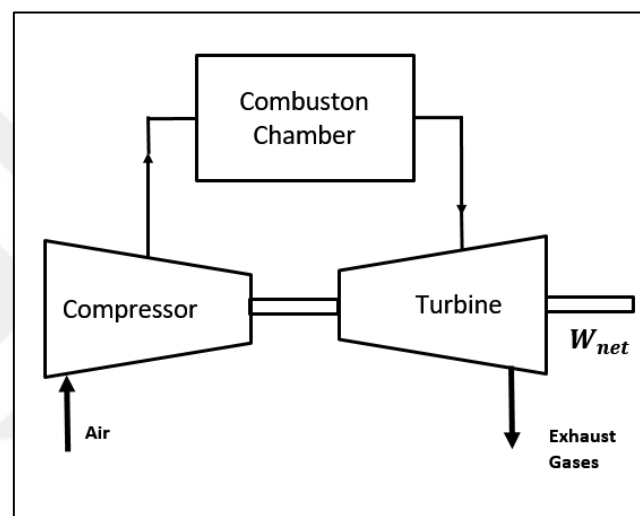


Figure 2.1. Schematic view of Brayton cycle

As the shaft starts to spin by an electric motor, pressurized air is delivered from the compressor to the combustion chamber. Fuel is sprayed through fuel nozzle and air swirler maintains fluid/fuel mixture, which is typically ignited by a capacitor-type ignitor.

The yield of burning, high momentum air leaves from the combustor, hits to turbine blades and starts to rotate the turbine rotor. Compressor and turbine modules both spin around the same driveshaft e.g. main shaft, which transmits a small part of the power from the turbine to compressor in order to provide continuous compression process. The rest of the momentum is used to maintain the required thrust to the aircraft in which the engine is mounted on. These types of engines are called as turbojets. The configuration, which has a fan in front of the engine is called as turbojet as well. An additional turbine module, which is attached to the aft, utilizes a part of the momentum of the working fluid in order to drive

the front fan. The main thrust is maintained by that fan. Turbojet engine was first developed by England and Germany before World War 2.

The turboprop engine was first developed in 1945 by Rolls Royce. The main difference from turbojets is having a propeller, which is attached to the aft of the turbine with a reduction gear. This configuration allows still having efficient propeller performance at a much slower speed than the operating shaft speed.

A turbofan engine is a compromise between turbojet and turboprop engines. The secondary airflow passes around the combustor, which allows additional thrust to be maintained.

Turboshaft engine utilizes high momentum exhaust gases in order to drive a shaft with a reduction gear rather than generating jet thrust. This type of engine is mostly used in helicopters.

There are typically two types of compressors, which are used in jet engines, are called axial and centrifugal compressors. In the case of having multiple stages, axial compressors have the capability of higher pressure ratio and higher efficiency than the centrifugal compressors[2]. Another advantage of axial type is the larger flowrate possible for the same inlet area. However multiple stages are required to achieve the desired pressure ratio whereas centrifugal-type compressors may need one stage to attain the same pressure ratio.

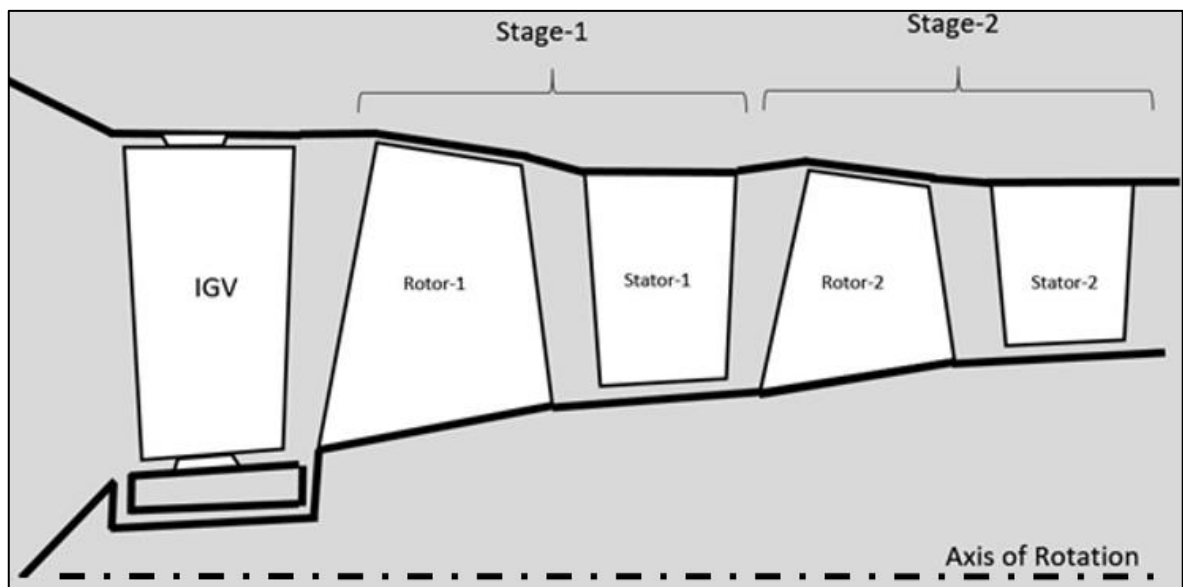


Figure 2.2. General view of an axial compressor

Basic axial compressor components are illustrated in Figure 2.2. Rotating first row is called as Rotor-1 and following stationary row is called as Stator-1. A stage consists of either a rotor row and a stator row.

The working fluid flow always tends to move back from high-pressure outlet to low-pressure inlet through compressor because of the adverse pressure gradient, which makes the design more difficult with increasing compression rate. In the rotor, the kinetic energy of working fluid is increased because the rotating blade leading edge interacts with the incoming air; therefore, the tangential velocity of the fluid increases. In addition to this, due to the diffusion process, which takes place at both rotor and stator, static pressure increases through the stages of the compressor. Attaining the desired compression rate entails having multiple stages are stacked successively through the compressor because the diffusion process has some limitations in its nature. Each stage has its own pressure ratio and adding more stages determines the overall pressure ratio. Figure 2.3 illustrates a top view of a compressor module. The throat width of the passage, which belongs to a couple of alongside blades or vanes, enlarges from leading-edge through the trailing-edge. Expanding flow passage decelerate flowing fluid and results in the diffusion process. This causes a rise in static pressure.

The working limits of the compressors are determined by choking and stall or surge. Choking occurs at a very high mass flow rate and low discharge pressure condition. At the low working speed of compressors, high-pressure ratio and exceeding of incidence angle of the blade results in early separation of flow around the airfoil. This stalled blade region cannot retain the pressurized downstream flow, which results in a complete compressor surge. This problem tends to occur at the speed that is far from the design point. To avoid this problem and increase stall range, inlet guide vane (IGV) is used. IGV guides the inlet flow and incorporates initial tangential velocity components to incoming air. Another way for avoiding surge is to deliver excessive pressurized air, which is larger than the blade couple can retain, into the atmosphere, therefore, reverse flow of fluid from outlet to inlet is prevented.

In early compressors, the flow was entirely subsonic and subsonic aerofoil profiles e.g. NACA were used in blade profiles [2]. Increasing flowrate and compression ratio demand forced the compressor designers to work with increased rotating shaft speed, which caused the flow passing through the blades supersonic. When this supersonic flow comes across

with a solid body, such as a blade or a vane leading edge, it would generate a shock. Therefore a certain amount of energy loss was encountered as the shock occurred. In order to maintain affordable efficiency while utilizing benefits of increased speed, some of the special aerofoil profiles such as double circular arc (DCA) (Figure 2.3), multiple circular arcs (MCA), S-Type or controlled diffusion aerofoil were used. Long chord aerofoils also maintain diffusion that takes place in a controlled manner. In brief, compressors, which have the working fluid Mach number varies around the transonic range is called as transonic compressors.

Several significant research was performed about transonic compressors [9 - 14]. When the incoming airflow with relative Mach number well below 1 arrives near to the leading edge of the blade tip section, flow accelerates and static pressure drop occurs due to curvature of the convex surface. That is the reason why it is called a suction surface. Acceleration occurs at 10-15 percentage of the chord from the leading edge which would make the flow supersonic and drops steadily until it reaches the subsonic range (Mach number below 0.8) at a later portion of the passage due to subsonic and supersonic diffusion. In transonic compressors, the leading edge of the blade is made sharp and less curvature is given so as to keep Mach number in the order of 1.2 around acceleration zone. In other words, acceleration is controlled utilizing from the geometric form of DCA, MCA, S-Type or controlled diffusion aerofoils. When the flow passes over the suction side due to less curvature effect of DCA blading and enlarging flow area, results in the flow to be decelerated. Therefore, flow becomes subsonic through blade passage.

In a transonic compressor, the flow, which goes through blade passages, is continuously transformed from supersonic to subsonic and subsonic to supersonic in passing through the blade passage in the chordwise direction. Furthermore, in the spanwise direction, flow can be subsonic near the hub region but it would go supersonic near the tip region due to relative velocity of the blade tip. The compressor, which has this type of transition, is also regarded as a transonic compressor.

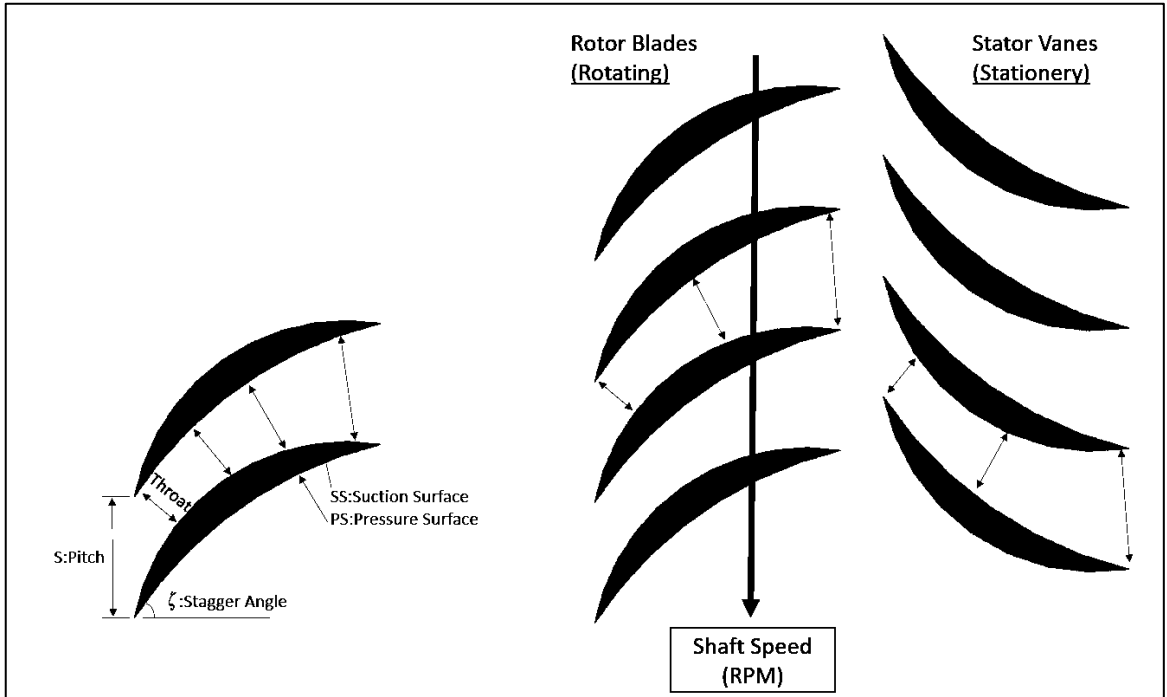


Figure 2.3. A general view for rotor and stator embodiment in a compressor stage

3. AXIAL COMPRESSORS MEAN LINE DESIGN

3.1. DEFINITION OF MEAN LINE DESIGN

Mean line design estimates the working fluid properties and velocities across the mean radius of the blades and vanes from the inlet through the outlet of the compressor. Some of the empirical corrections are introduced by collected experimental data belong to specific aerofoil shapes. Calculations are done on mean line region utilizing steady-state energy equation.

Basically, the stagnation enthalpy change is expressed as constant specific heat ideal gas stagnation temperature change and conservation of momentum (Tangential velocity change). Then the estimated air angles are projected to the hub and tip regions by utilizing the radial equilibrium equations. Inlet and outlet angles of blade sections are determined by utilizing deviation and incidence angles.

While basic aerofoil shapes and the shaft speed are determined, mechanical calculations should be carried on simultaneously. The most critical mechanical failure sources blade centrifugal stress at hub location and sudden fracture because of resonance. Natural frequencies should be calculated carefully so as to maintain compressor structural integrity. Minimizing the size and the blade root stress, high efficiency and compression ratio at the same time keeping the blade natural frequency at a specified range should be the objectives of the optimization process.

3.2. AERODYNAMIC DESIGN OF AXIAL COMPRESSOR

3.2.1. Thermodynamic Calculations in an Axial Compressor Stage

A compressor stage consists of a blade row that rotates about the engine axis at a specified RPM and it is followed by a stator vane row which is stationary. Inlet air arrives at the rotor blade leading edge, then accelerates due to the tangential velocity component of rotor blades until it travels to the trailing edge of the blade. This effect increases the kinetic energy of the

working fluid. At the stator vane passage, deceleration occurs because the expansion of working fluid and attained kinetic energy of the fluid is transformed into an increase in static pressure.

Axial compressors typically have successive stages so as to increase the overall pressure of working fluid because single-stage pressure building capacity is limited due to adverse pressure gradient through the inlet of the compressor.

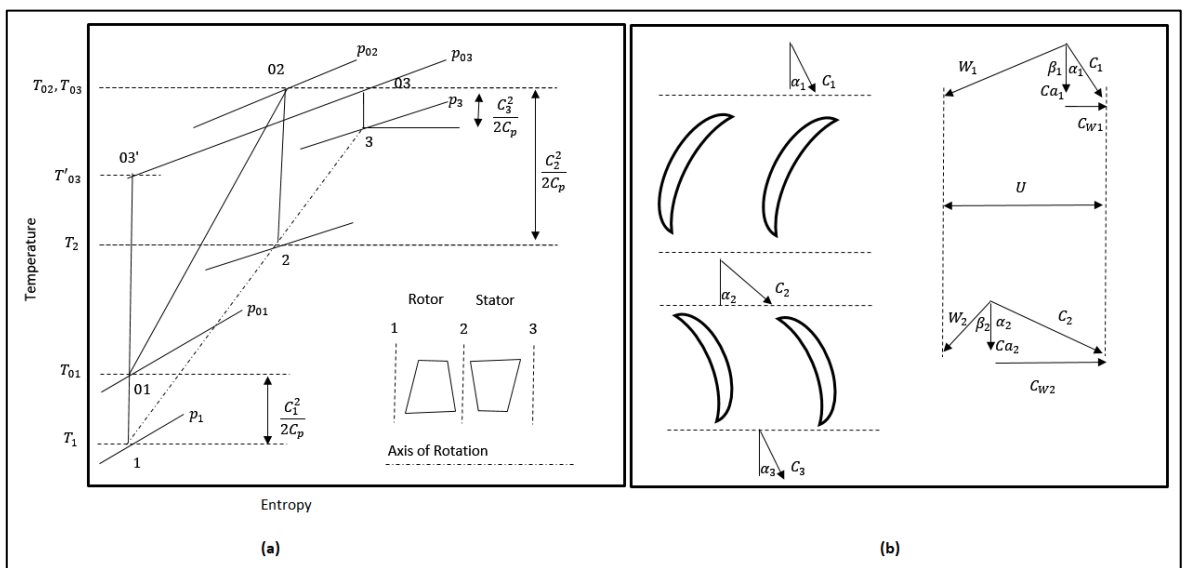


Figure 3.1. T-s and velocity diagram of a stage. (a) T-s diagram, (b) Velocity triangles

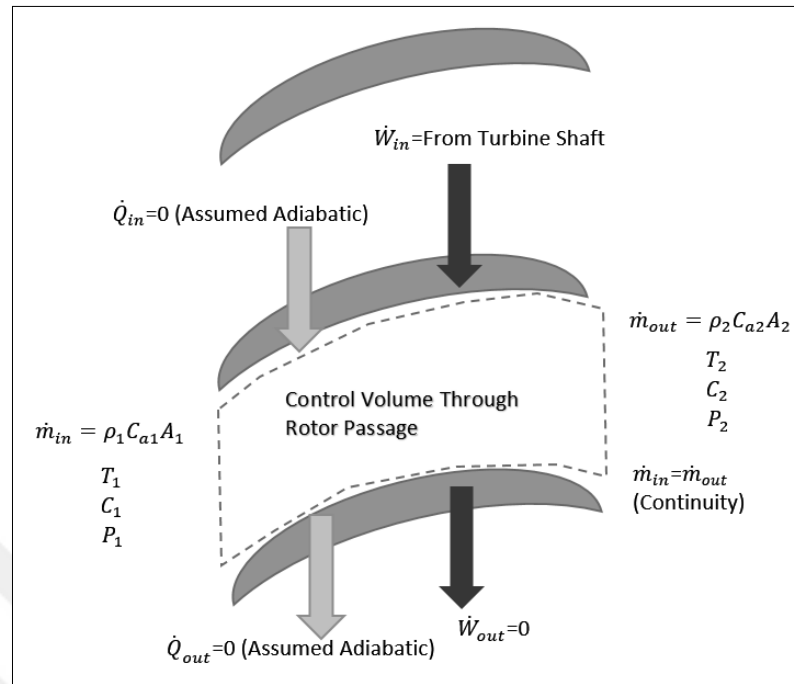


Figure 3.2. Control volume through rotor passage

In mean line design, the basic steady flow energy equation is applied to the rotor. The rate of net energy transfer equals "0" because of the steady process. From the first law of thermodynamics,

$$\dot{E}_{in} - \dot{E}_{out} = \frac{dE_{system}}{dt} = 0 \quad (3.1)$$

$$\dot{Q}_{in} + \dot{W}_{in} + \dot{m} \left(h_1 + \frac{C_1^2}{2} + gz_1 \right) = \dot{Q}_{out} + \dot{W}_{out} + \dot{m} \left(h_2 + \frac{C_2^2}{2} + gz_2 \right) \quad (3.2)$$

Recalling that, $h_{01,02} = h_{1,2} + \frac{C_{1,2}^2}{2}$ and $\dot{Q} = \dot{m}q$, $\dot{W} = \dot{m}w$.

$$q_{in} + w_{in} + (h_{01} + gz_1) = q_{out} + w_{out} + (h_{02} + gz_2) \quad (3.3)$$

Change in elevation is ignored through the compressor ($\Delta z = 0$) because its effect is negligible compared to other contributors. Then steady flow equation becomes as follows,

$$q_{in} + w_{in} + h_{01} = q_{out} + w_{out} + h_{02} \quad (3.4)$$

The compression process is assumed to be adiabatic. Therefore both $\dot{Q}_{in} = \dot{Q}_{out} = 0$. For the compressor, there is a turbine shaft work that drives the compressor rotor. $w_{in} + h_{01} = h_{02}$ or $\dot{W}_{in} + \dot{m}h_{01} = \dot{m}h_{02}$.

For a calorically perfect gas, specific heats do not change with respect to temperature. Therefore, total enthalpy is given in terms of c_p and total temperature,

$$h_{01} = c_p T_{01}, h_{02} = c_p T_{02} \quad (3.5)$$

Variation in c_p around related temperature range is ignored [2]. Therefore, the power input in order to drive the compressor rotor is given as follows:

$$\dot{W}_{in} = \dot{m}c_p(T_{02} - T_{01}) \quad (3.6)$$

From Euler Turbomachinery Equation, rate of work in (Power) is also written as follows:

$$P = \tau\omega = \omega\dot{m}(r_2 C_{w2} - r_1 C_{w1}) = \dot{W}_{in} = \dot{m}(U_2 C_{w2} - U_1 C_{w1}) \quad (3.7)$$

Where " U " stands for the blade tangential velocity and " C_w " stands for the fluid tangential velocity as seen in Figure 3.1. For convenience, " \dot{W} " stands for the work rate into the compressor shaft that will be used instead of " \dot{W}_{in} ", " w " stands for the work to the compressor shaft per unit mass that will be used instead of " w_{in} ". Utilizing velocity triangles (Figure 3.1.b) equation 3.7 is written in terms of axial velocities:

$$\dot{W} = \dot{m}(U_2 C_{a2} \tan \alpha_2 - U_1 C_{a1} \tan \alpha_1) \quad (3.8)$$

Where " C_a " stands for the fluid axial velocity and " α " stands for the angle between axial direction and absolute velocity of incoming fluid. The T-s diagram of a compressor stage (Figure-3.1.a) illustrates that the temperature and pressure relationship and losses. The total pressure is increased only in the rotor because the turbine output work is applied to the compressor shaft directly via the main shaft. The stator only transforms kinetic energy to an increase in static pressure while the stagnation (Total) temperature remains constant. In other words, total enthalpy does not change in the diffuser, only static enthalpies changes. In actual working conditions, because of the frictional losses, total pressure decreases in the stator [15,16].

During the mean line (1D) analysis the calculations are performed at the mean height of the blades. U is taken as the tangential speed of the blade. Velocity vectors are illustrated in Figure 3.1. C_1 stands for incoming air velocity (Absolute). It has an angle of α_1 relative to the axial direction. The resultant velocity vector of C_1 and U (Blade speed in a tangential plane) is nothing but the relative velocity W_1 of incoming air with respect to rotating blade.

Absolute velocity increases right after passing through the rotor blade passage. Utilizing trigonometry, C_2 stands for the absolute velocity at the rotor exit can now be calculated. C_2 is diffused to C_3 (Decelerated) at diffuser passage. Inlet and outlet absolute velocity magnitudes C_1 , C_3 and their relevant angles α_1 , α_3 values do not vary significantly [2].

3.2.2. The Factors Which Affect Pressure Ratio

One of the main design objectives of an axial compressor is to maintain the required pressure ratio for the combustor to be operated. There are important factors, which affect the value of the pressure ratio and they should be considered in the design process.

From velocity triangles diagram $\tan \beta_1$ and $\tan \beta_2$ are written as follows:

$$\tan \beta_1 = \frac{U_1 - C_{w1}}{C_{a1}} \quad (3.9)$$

$$\tan \beta_2 = \frac{U_2 - C_{w2}}{C_{a2}} \quad (3.10)$$

The useful work which is given into the compressor shaft is transformed into a stagnation temperature rise [2]. Then equation 3.2 is written as follows:

$$w = \Delta T_{0S} = \frac{U_2 C_{w2} - U_1 C_{w1}}{c_p} = \frac{U_2^2 - U_1^2 + U_1 C_{a1} \tan \beta_1 - U_2 C_{a2} \tan \beta_2}{c_p} \quad (3.11)$$

From equation 3.11 it is seen that stagnation temperature rise increases as the tangential blade speed increases. High axial velocity and high fluid deflection " $\beta_1 - \beta_2$ " both increase the stagnation temperature.

On the other hand, there are some limiting conditions for the above parameters. Such as high blade tangential velocity " U " that results in high centrifugal blade root stress which will be detailed more in the "Mechanical Design" chapter.

At rotor inlet high absolute velocity " C " in conjunction with high tangential blade velocity " U " cause the maximum relative velocity " W " occurs at tip region by Pythagorean theorem $W^2 = U^2 + C^2$. In case of not having IGV at the inlet of the compressor, absolute velocity becomes pure axial velocity [2]. Thus, inlet static temperature is expressed as follows:

$$T_1 = T_{01} - \frac{c_1^2}{2c_p} \quad (3.12)$$

At " T_1 " static temperature, local acoustic velocity " c " is expressed as follows:

$$c = \sqrt{\gamma RT_1} \quad (3.13)$$

Relative Mach number is then expressed as follows at the calculated acoustic velocity:

$$(Mach_{1,rel})_{tip} = \frac{(W_1)_{tip}}{c} \quad (3.14)$$

Axial velocities are varying between 150 to 200 m/s for industrial gas turbines [2]. In the meantime, Mach number variation is between 0.2 to 2.5 [17] across the compressor. It is also known that up to about 1.1 transonic Mach numbers do not result in excessive losses [2]. Therefore it can be stated that high axial velocity is limited by Mach number in order to avoid excessive losses to occur at the compressor stage.

High deflection " $\beta_1 - \beta_2$ " is maintained by reducing β_2 for considering at constant β_1 . The angle β_2 is the angle between relative velocity W_2 vector and axial direction. Reducing β_2 results in reducing W_2 (Figure 3.1) which means diffusion takes place. The high rate of diffusion is limited and some of the criteria such as "de Haller" number and "Diffusion Factor" are presented and detailed more in the following sections [2].

3.2.3. Radial Equilibrium in a Fluid Element

Due to the centrifugal effect, there is a radial force component, which arises on a fluid element. There are three sources of that centrifugal effect,

- Circular motion on the plane that is perpendicular to rotation axis (Aft looking forward or forward-looking aft directions),

- The circular motion along the radius in meridional plane because of the streamline curvature (Profile view),
- The third one is due to the radial component of linear acceleration along the streamline (Profile view) Fig.8.

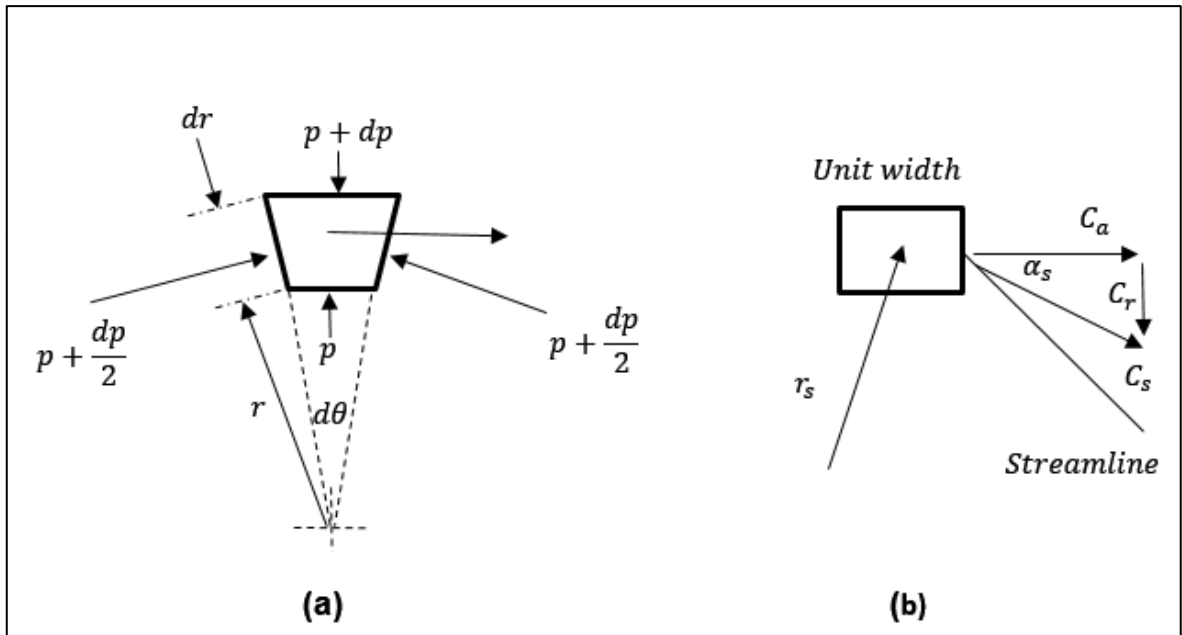


Figure 3.3. Force balance on a fluid element in a flow passage. (a) Forward-looking aft or aft looking forward view, (b) Meridional view (Profile view) [2]

A fluid element has a unit width and density ρ , the mass of the element is expressed as follows:

$$m = \rho r dr d\theta \quad (3.15)$$

Centrifugal force acts on a fluid element in two planes. F_1 is acting in the plane which is perpendicular to the rotation axis, F_2 and F_3 is in the meridional plane (Streamline plane). They are both radial forces. Gravitational force is ignored because of having a very small magnitude corresponding to others [2].

$$F_1 = (\rho r dr d\theta) \frac{C_w^2}{r} \quad (3.16)$$

$$F_2 = (\rho r dr d\theta) \frac{C_s^2}{r_s} \cos \alpha_s \quad (3.17)$$

Suffix ‘‘S’’ indicates that the associated parameter belongs to streamline. Final inertial force component arises due to acceleration along the streamline and expressed as follows:

$$F_3 = m \frac{dc_S}{dt} \sin \alpha_S = (\rho r dr d\theta) \frac{dc_S}{dt} \sin \alpha_S \quad (3.18)$$

F_1, F_2, F_3 forces are in the radial direction, therefore they are combined into one equation,

$$F_{Radial} = (\rho r dr d\theta) \left[\frac{c_w^2}{r} + \frac{c_s^2}{r_s} \cos \alpha_S + \frac{dc_S}{dt} \sin \alpha_S \right] \quad (3.19)$$

Pressure force balance on fluid element is expressed as follows:

$$F_{Pressure} = (p + dp)(r + dr)d\theta - prd\theta - 2 \left(p + \frac{dp}{2} \right) dr \frac{d\theta}{2} \quad (3.20)$$

Neglecting second-order terms and equating both equations F_{Radial} and $F_{Pressure}$ yields radial equilibrium equation as follows:

$$\frac{1}{\rho} \frac{dp}{dr} = \frac{c_w^2}{r} + \frac{c_s^2}{r_s} \cos \alpha_S + \frac{dc_S}{dt} \sin \alpha_S \quad (3.21)$$

r_s value is large enough to assume α_S so small [2], radial equilibrium equation becomes,

$$\frac{1}{\rho} \frac{dp}{dr} = \frac{c_w^2}{r} \quad (3.22)$$

Stagnation enthalpy along the span is h_0 . The absolute velocity C is as follows,

$$h_0 = h + \frac{C^2}{2} = h + \frac{1}{2}(C_a^2 + C_w^2) \quad (3.23)$$

Enthalpy change along span with respect to change in r is given by:

$$\frac{dh_0}{dr} = \frac{dh}{dr} + C_a \frac{dC_a}{dr} + C_w \frac{dC_w}{dr} \quad (3.24)$$

Gibb's relation is applied and both equations are combined that gives the following equation by omitting second-order terms:

$$\frac{dh_0}{dr} = T \frac{ds}{dr} + \frac{1}{\rho} \frac{dp}{dr} + C_a \frac{dC_a}{dr} + C_w \frac{dC_w}{dr} \quad (3.25)$$

Combining with Eqn.3.24 gives vortex energy equation by dropping the entropy gradient along the span,

$$\frac{dh_0}{dr} = C_a \frac{dC_a}{dr} + C_w \frac{dC_w}{dr} + \frac{C_w^2}{r} \quad (3.26)$$

When the constant specific work is desired through the span $\frac{dh_0}{dr} = 0$ and equation reduces to

$$C_a \frac{dC_a}{dr} + C_w \frac{dC_w}{dr} + \frac{C_w^2}{r} = 0 \quad (3.27)$$

And axial velocity distribution is assumed to be 0 along with the span yields,

$$\frac{dC_w}{C_w} = -\frac{dr}{r} \quad (3.28)$$

After integration,

$$C_w r = \text{constant} \quad (3.29)$$

This is known as free vortex condition, whirl velocity varies inversely with respect to radius.

3.2.4. Annulus Types of Axial Compressor

Generally, three basic types of annulus shapes of compressors are present as illustrated in Figure 3.4. Constant hub diameter compressors are usually found in industrial applications. This type of shape serves greater outer space than the other types do. That may be accounted as an advantage to maintain an allowance for accessories and external equipment to be mounted on. Due to smaller disk rim diameter corresponding to other types, constant disc hub diameter design has another advantage because of lower manufacturing costs and rim stress [5]. Aerodynamic losses are less than that for constant tip design. Descending the mean radius results in lower tip speed at later stages; therefore, higher loaded blades [4], more number of stages are required with respect to constant tip and mean design.

Constant mean diameter compressors have a straight mean diameter along the flow path. It provides easier calculation steps compared to the constant tip and hub design.

Constant tip compressors have a constant diameter size at tip or casing location. It is usually used in aircraft and missile engines. Mean diameter increases per stage numbers, eventually tangential speed increases. Temperature rise increases at later stages as well. Therefore less

number of stages are required to obtain a given pressure ratio. Other advantages are less fluid deflection requirement and an increase in de Haller number [2]. On the other hand, relatively higher end-wall losses, higher disk stresses and small volume for externals (External equipment) are some of the disadvantages [3].

An additional annulus shape, which is called variable mean line, is a compromise among constant tip, hub and mean diameter annulus shapes. When customer requirements force designers to limit or restrict some of sizing parameters, variable mean line design in conjunction with optimization methods is an option to find optimum design point.

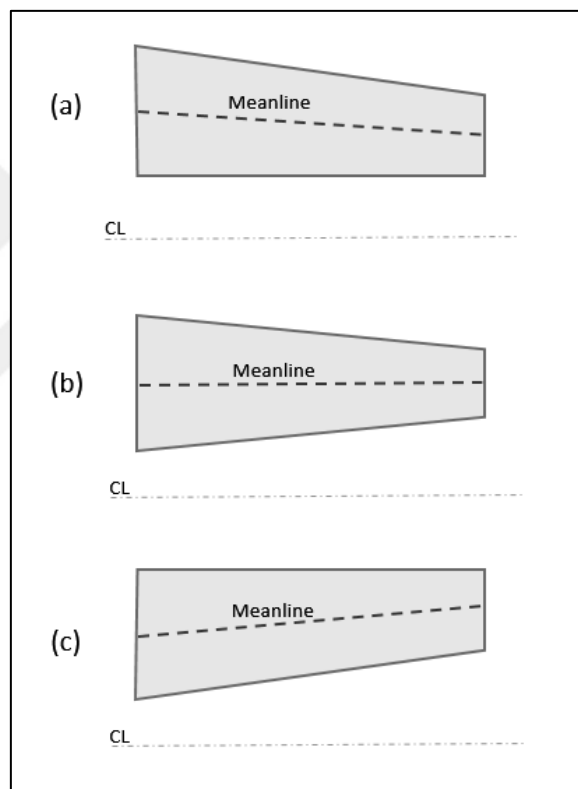


Figure 3.4. Annulus types. (a) Constant Hub Radius, (b) Constant Mean Radius, (c) Constant Tip Radius

In the ACMC tool, the designer can choose any of four annulus shapes via constraining desired size parameters.

3.2.5. Blockage and Work Done Factor

Through the blade and vane passages, boundary layer thickening occurs in the direction of the flow due to the adverse pressure. In addition to this, tip leakage contributes to the thickening effect. Radial distribution of axial velocity varies along the span because of local narrowing and widening of flow area. In other words, local acceleration and deceleration of axial velocity occur at flow passage along the span. Typical axial velocity distribution along the span is illustrated in Figure 3.5 for the first and fourth stages of a compressor.

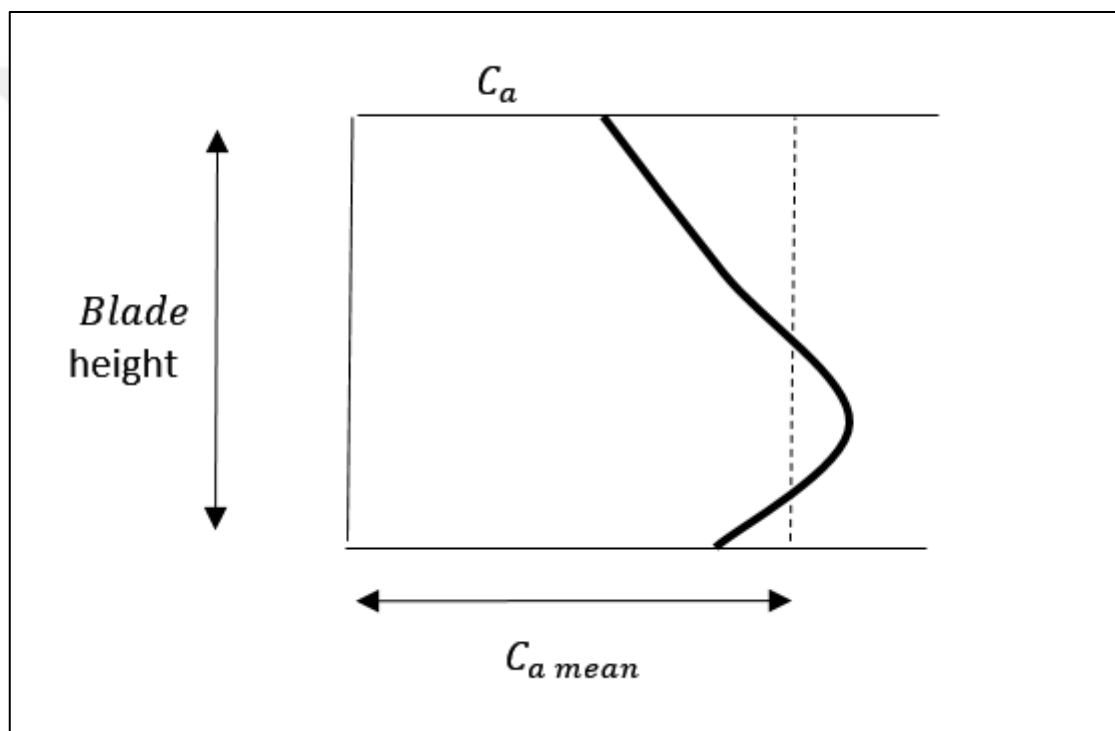


Figure 3.5. Variation in the axial velocity of the fluid along the span [2]

Due to the complex nature of boundary layer thickening effects, calculations are not practical; thus, there are empirical correlations based on compressor test data which are utilized [2]. Stagnation temperature rise and work-absorbing capacity are less than calculated from equation 3.6. Therefore, an empirical parameter i.e. work done factor " λ " is incorporated to the expression. Work done factor is less than unity. " λW " gives the actual work which is given to the stage.

Applying " λ " to stagnation temperature rise then expression becomes:

$$w = \Delta T_{0S} = \frac{\lambda(U_2 C_{w2} - U_1 C_{w1})}{c_p} = \frac{\lambda(U_2^2 - U_1^2 + U_1 C_{a1} \tan \beta_1 - U_2 C_{a2} \tan \beta_2)}{c_p} \quad (3.30)$$

The mean work done factor with respect to the number of stages is given in Figure 3.6. A fourth-order polynomial is introduced to the ACOM program.

An alternative approach, "Blockage Factor" is an American design practice. The blockage factor approach deals with reducing the effective annulus area by the growth in boundary layer thickness. Both approaches represent empirical corrections [2] and have the same effect on calculations. If the work-done factor is used there is no need to use blockage factor.

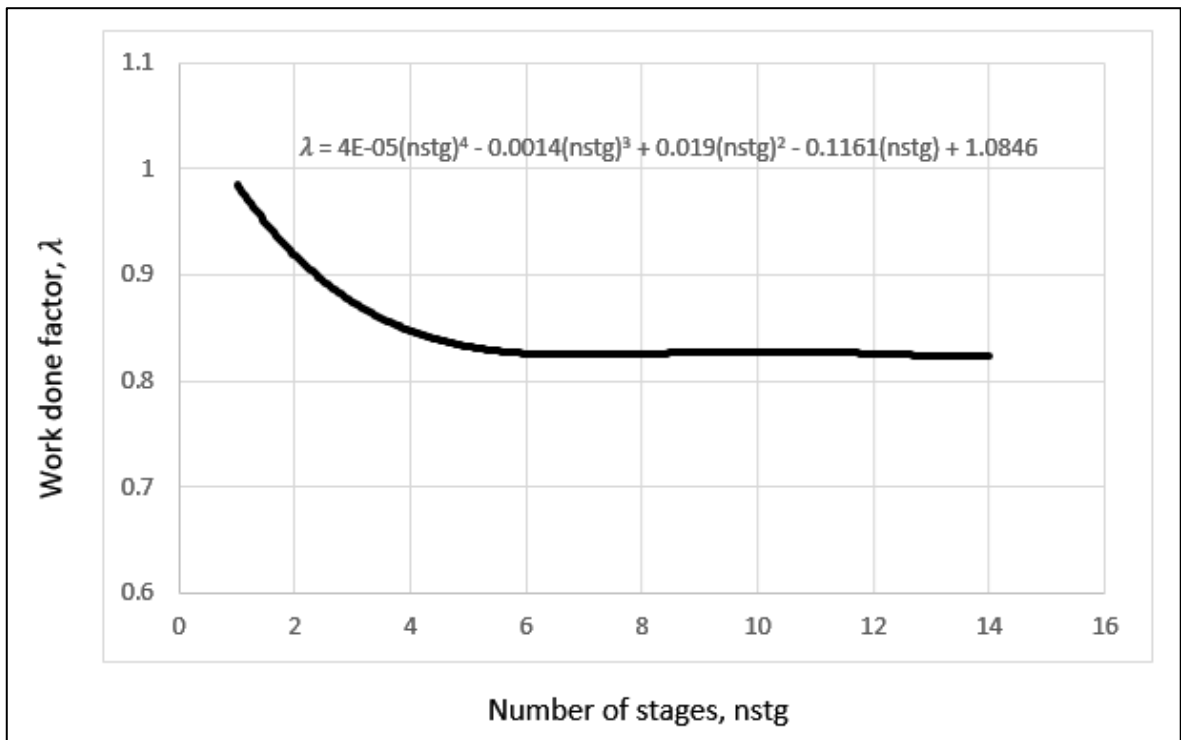


Figure 3.6. Mean work done factor with respect to the number of stages

3.2.6. Degree of Reaction

In an axial compressor stage, both rotor and stator contribute to static pressure rise due to diffusion. Degree of Reaction is the ratio of static enthalpy rise in the rotor to the static enthalpy rise in the whole stage.

Degree of reaction is defined as follows:

$$\Lambda = \frac{\text{static enthalpy rise in the rotor}}{\text{static enthalpy rise in the stage}} = \frac{h_2 - h_1}{h_4 - h_1} \quad (3.31)$$

The degree of reaction can be expressed in terms of static temperature rise for convenience as well. In a stage, static temperature rise equals to total temperature rise $\Delta T_S = \Delta T_{0S}$ by the assumption of constant axial velocity in conjunction with inlet and outlet absolute velocities; thus, work is expressed as follows:

$$w = c_p(\Delta T_{rotor} + \Delta T_{stator}) = c_p \Delta T_S \quad (3.32)$$

$$w = c_p \Delta T_S = c_p \Delta T_{0S} = U_2 C_{a2} \tan \alpha_2 - U_1 C_{a1} \tan \alpha_1 \quad (3.33)$$

All work input is consumed by the rotor, therefore work can be expressed in terms of static temperature and absolute velocity change,

$$w = c_p \Delta T_{rotor} + \frac{1}{2}(C_2^2 - C_1^2) \quad (3.34)$$

Combining Eqn. 3.33 and 3.34 yields,

$$c_p \Delta T_{rotor} = U_2 C_{a2} \tan \alpha_2 - U_1 C_{a1} \tan \alpha_1 - \frac{1}{2}(C_2^2 - C_1^2) \quad (3.35)$$

From the velocity triangles,

$$C_2 = C_{a2} \sec \alpha_2 \quad (3.36)$$

$$C_1 = C_{a1} \sec \alpha_1 \quad (3.37)$$

Eqn. 3.36 and 3.37 are introduced to Eqn. 3.35,

$$c_p \Delta T_{rotor} = U_2 C_{a2} \tan \alpha_2 - U_1 C_{a1} \tan \alpha_1 - \frac{(C_{a2}^2 \tan^2 \alpha_2 - C_{a1}^2 \tan^2 \alpha_1 + C_{a2}^2 - C_{a1}^2)}{2} \quad (3.38)$$

Then, the degree of reaction becomes:

$$\Lambda = 1 - \frac{0.5(C_{a2}^2 \tan^2 \alpha_2 - C_{a1}^2 \tan^2 \alpha_1 + C_{a2}^2 - C_{a1}^2)}{U_2 C_{a2} \tan \alpha_2 - U_1 C_{a1} \tan \alpha_1} \quad (3.39)$$

Eqn. 3.39 defines the degree of reaction. Due to the fact that flow deceleration through each flow passage belongs to the rotor and stator, the static pressure gradient takes place across

the stage. Adverse pressure gradient results in boundary layer separation. It would be preferred that equal distribution of static pressure or enthalpy rise between each rotor and stator pairs belong to a stage. This is called symmetrical blading. But it is not necessary.

In the case of using IGV, positive α_1 magnitude reduces the degree of reaction. That means the contribution of the rotor to the static enthalpy rise is diminished. Moreover, it also reduces the inlet relative velocity. Thus inlet relative Mach number is reduced. Conversely, the contribution of the stator to the static enthalpy rise and stator entrance relative Mach number is increased.

The compressor inlet without IGV results in $\alpha_1 = 0$; thus, a high degree of reaction and high inlet Mach number is expected.

3.2.7. Pitch to Chord Ratio, Hub to Tip Ratio, and Aspect Ratio

Pitch to cord ratio (s/c) is the ratio of "s", which stands for the distance between adjacent blades, and "c" stands for the chord length. The inverse of that (c/s) is known as solidity which is preferred in American design practice. Pitch to cord ratio is basically used for determining incidence and deviation angles which will be given in detail in the following section. Small values of the pitch to cord ratio means that "s" is smaller corresponding to "c". An increase in the number of blades results in getting smaller "s" values. The high number of blades causes an increase in the blade surface area of a certain stage. Thus friction and profile losses increase.

$$s = \frac{2\pi r}{NB} \quad (3.40)$$

Hub to tip ratio (HTR) is the ratio of hub radius over the tip radius. Preliminary design starts with the value of HTR usually 0.5 [2]. It varies from 0.4 to 0.7 [5]. At the inlet of the compressor, the high HTR causes a drop in efficiency. Due to the nature of the compressor, near the exit stages, the blade heights are already low. In other respects, high HTR near the exit stages results in smaller blades. This may cause an increase in end-wall losses.

$$HTR = \frac{r_{hub}}{r_{tip}} \quad (3.41)$$

Aspect ratio (AR) is the ratio of blade height "h" over the chord length "c". The value of 3 is a good start for preliminary design [2], but lower values up to 1.4 are suitable for advanced design steps. Chord length is determined by this ratio then imposed into PCR formulation. The trends in aspect ratio are to use lower values in order to attain higher stage efficiency and stall margin, improved performance at high Mach number condition, improved performance at higher diffusion factors and higher incidences [5]. Aspect ratio formulation is given by,

$$AR = \frac{h}{c} \quad (3.42)$$

In addition to those mentioned benefits utilizing a lower aspect ratio may result in fewer stages which are required so as to attain a given overall pressure ratio.

3.2.8. Diffusion Factor (DF) and De Haller (DH) Criterion

The diffusion factor was defined by Lieblein [18] in order to establish a related loading parameter to express the total diffusion on the blade suction surface since the boundary layer on the suction surface was recognized as limiting the pressure rise and turning of the blades. For a 2D blade section diffusion factor is expressed as follows:

$$DF = 1 - \frac{W_2}{W_1} + \frac{|r_1 C_{w1} - r_2 C_{w2}| s}{(r_1 + r_2) W_1 c} \quad (3.43)$$

In equation 3.43 as the tangential velocity (C_w) change was increased, which means the loading of the corresponding section is increased as well.

Diffusion factor is one of the major limiting parameters in compressor design where DF values of exceeding 0.6 might be the blade stall inception value, which should be avoided. 0.45 is taken as the typical design value as a limit [19].

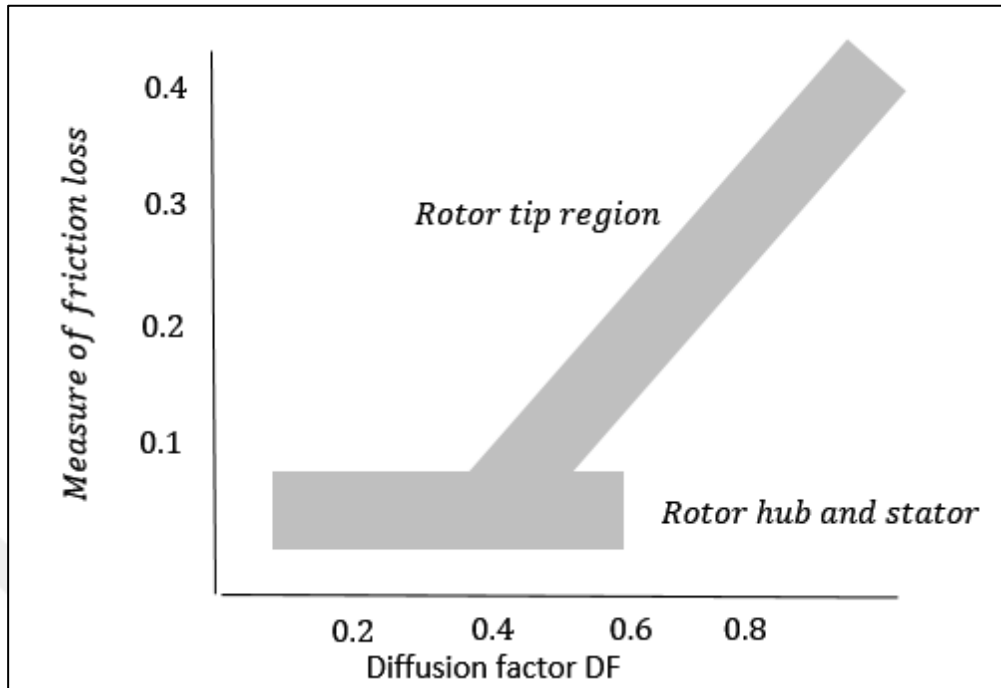


Figure 3.7. Variation of frictional losses with respect to diffusion factor [2]

Detailed design values of DF with respect to frictional losses were obtained from several NACA tests illustrated in Figure 3.7. In the ACOM program, the Diffusion factor limit for the tip section was taken as 0.4, for the mean line 0.43 and for the hub section 0.48. Those values are slightly lower than the values which are shown in Figure 3.7 because of providing an allowance for the unpredicted effects of the preliminary design process.

On the other hand, maximum suction surface velocity and wake parameters are generally unknown. Lieblein [18] derived a more general correlation which is called equivalent diffusion factor, which is expressed as follows:

$$DF_{eq} = \frac{\cos \beta_2}{\cos \beta_1} \left[1.12 + 0.61 \cos \beta_1^2 (\tan \beta_1 - \tan \beta_2) \frac{s}{c} \right] \quad (3.44)$$

In Figure 3.8, at minimum loss incidence angle, exceeding DF_{eq} value of 2, results in a rapid increase in losses. The value 2 for DF_{eq} can also be imposed on to ACOM tool as a limiting factor.

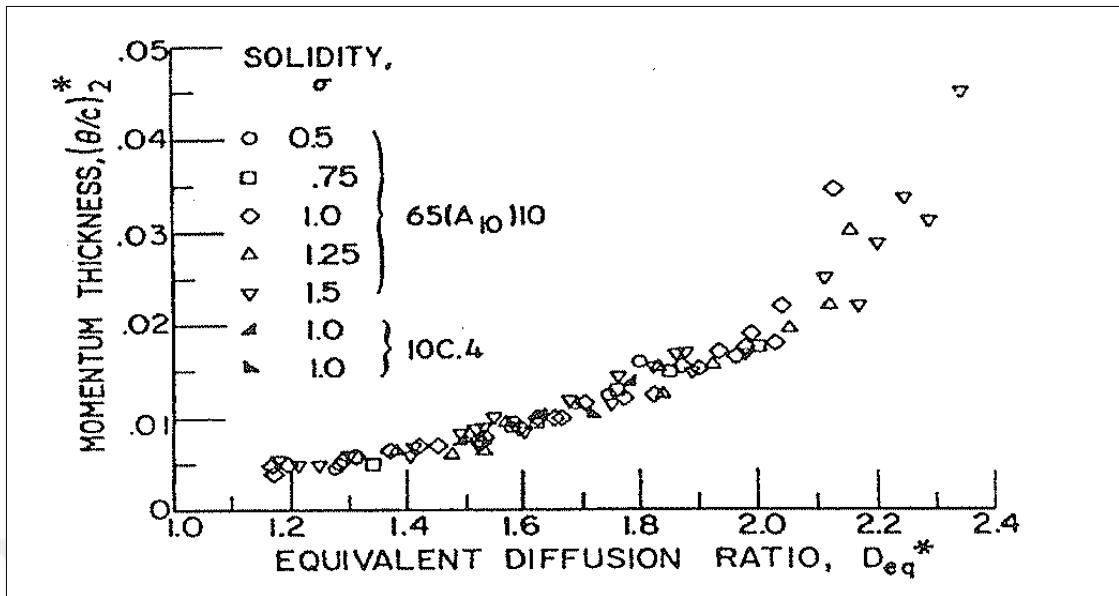


Figure 3.8. Correlation of wake momentum thickness with an equivalent diffusion factor at a minimum loss incidence angle [20]

De Haller (DH) criterion is another detection way to stall inception. It is defined as the ratio of exit absolute velocity to inlet absolute velocity. Figure 3.9 illustrates relative velocity distribution over the suction and pressure surfaces of the blade. Too low values of exit velocity corresponding to the inlet is a sign of stall inception. The calculated value should be greater than 0.72 [2]. The formulation for DH is expressed as follows:

$$DH = \frac{w_2}{w_1} \quad (3.40)$$

In order to increase blade loading, de Haller number will be slightly reduced to 0.69 in this study. The velocities, which are used in diffusion calculations, are determined based on if the calculations that are carried on rotor or stator. For blade calculations, the relative velocity is used, for vane calculations, absolute velocity is used.

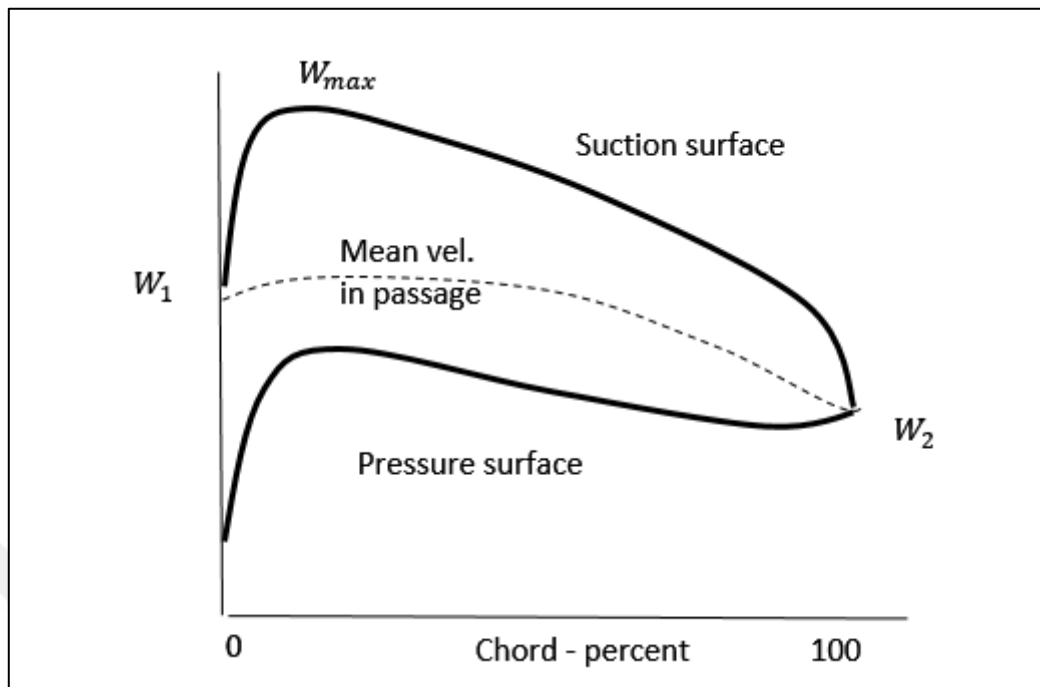


Figure 3.9. Relative velocity distribution over suction and pressure surfaces of blade [2]

3.2.9. Cascade Notation, Incidence and Deviation Calculations

A simple cascade test setup is illustrated in Figure 3.10. Cascade tests are performed in order to determine incidence and deviation angles for a specific aerofoil shape with respect to static pressure variation. The test is conducted for over several incidence angles of the air which enters the cascade. Velocity and pressure measurement is performed via a pitot tube. The difference between the incoming air angle α_1 and blade air receiving metal angle α_1' is denoted as i which is called incidence angle and expressed as follows:

$$i = \alpha_1 - \alpha_1' \quad (3.46)$$

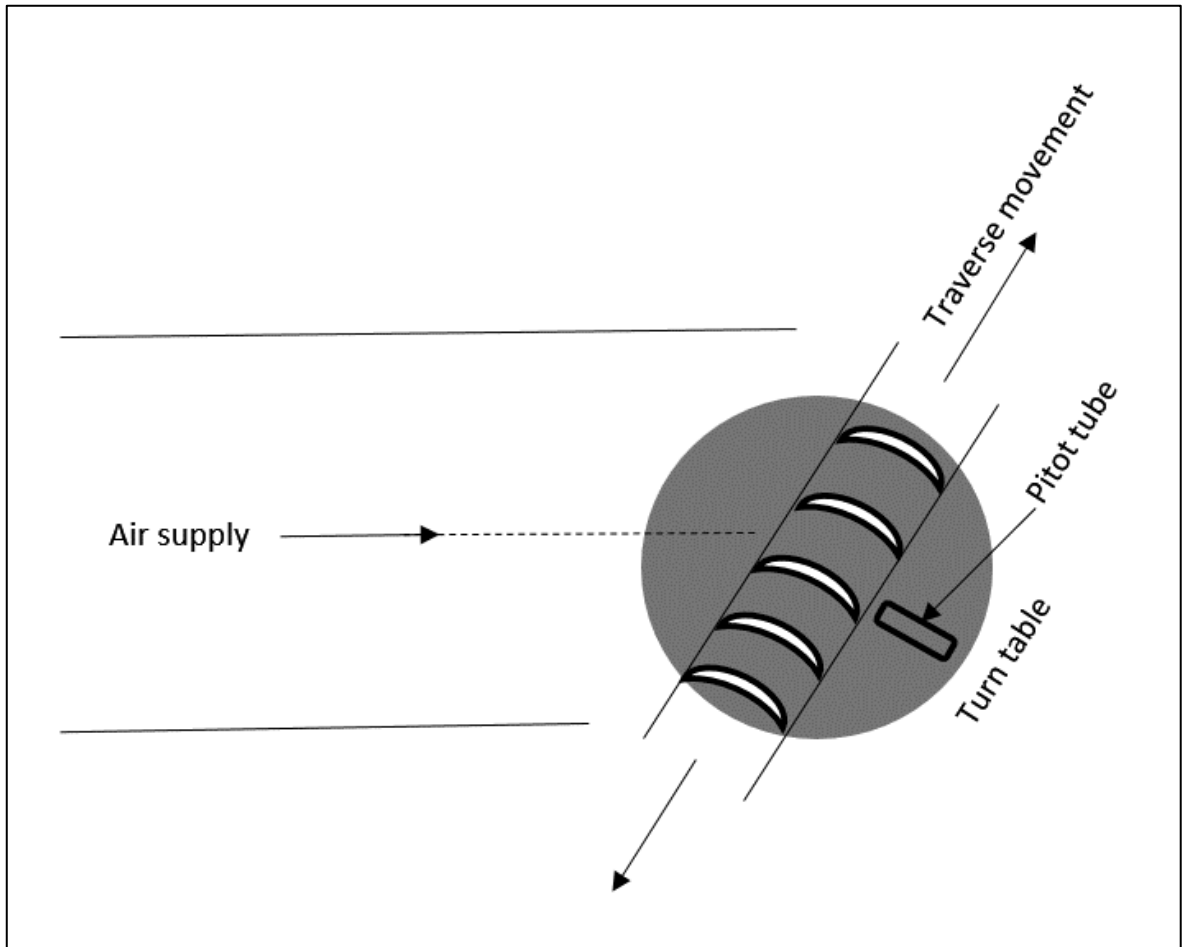


Figure 3.10. Simple cascade test setup [2]

Due to the fact that blades in the cascade setup are not rotating, instead of relative air angles β , absolute air angles α are used in formulations and the notation. In Figure 3.10 cascade notation is illustrated.

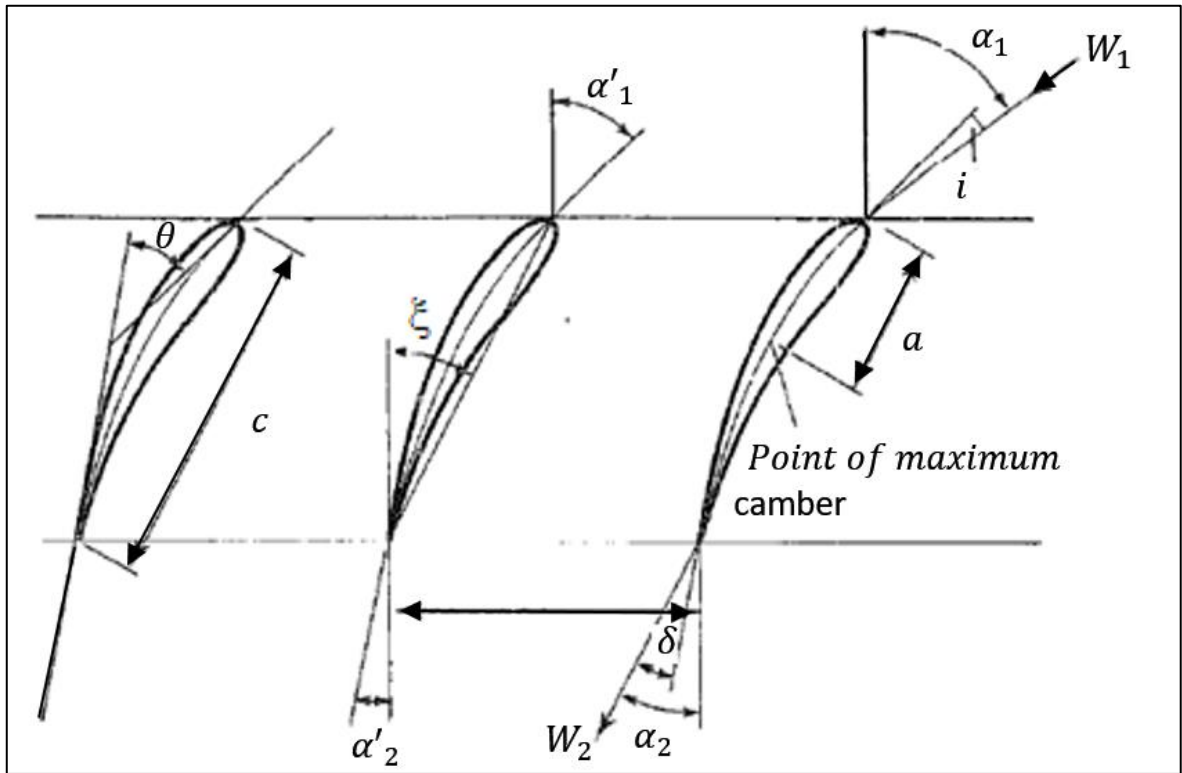


Figure 3.11. Cascade test aerofoil notation [2]

On the other hand, air leaving angle from the cascade aerofoil trailing edge is now denoted as α_2 . The corresponding metal angle is denoted as α_2' . Thus deviation angle is expressed as follows:

$$\delta = \alpha_2 - \alpha_2' \quad (3.47)$$

In the cascade test setup beside angular orientation, the Pitot tube can be translated in the transverse direction. At this time the aerofoil trailing edge stagnation pressure loss distribution and deflection angles ε can now be plotted as in Figure 3.11. Since the loss is related with the inlet velocity, for the convention it is expressed as a dimensionless form which is expressed as follows:

$$loss = \frac{P_{01} - P_{02}}{0.5\rho W_1^2} = \frac{\omega}{0.5\rho W_1^2} \quad (3.48)$$

$$\varepsilon = \alpha_1 - \alpha_2 \quad (3.49)$$

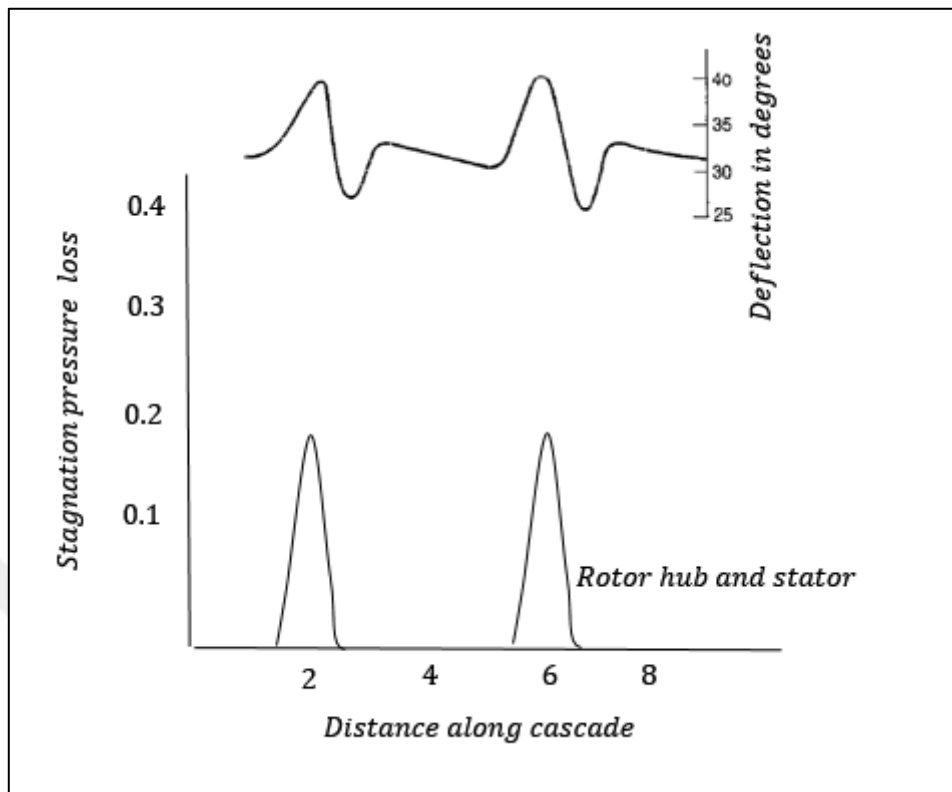


Figure 3.12. Variation of stagnation pressure loss and deflection for cascade at a certain incidence [2]

Finally, the tests are performed for several values of incidence angles and the results are collected into a form that is constituted by mean loss and mean deflection as shown in Figure 3.12.

From equation 3.11, if the deflection is kept high as much as possible; therefore, stagnation temperature rise would be high. But after a certain value, high deflection might cause a rapid increase in losses because of the stall (Diffusion factor limit).

The design incidence angle should be in a region where the mean stagnation loss curve becomes flat.

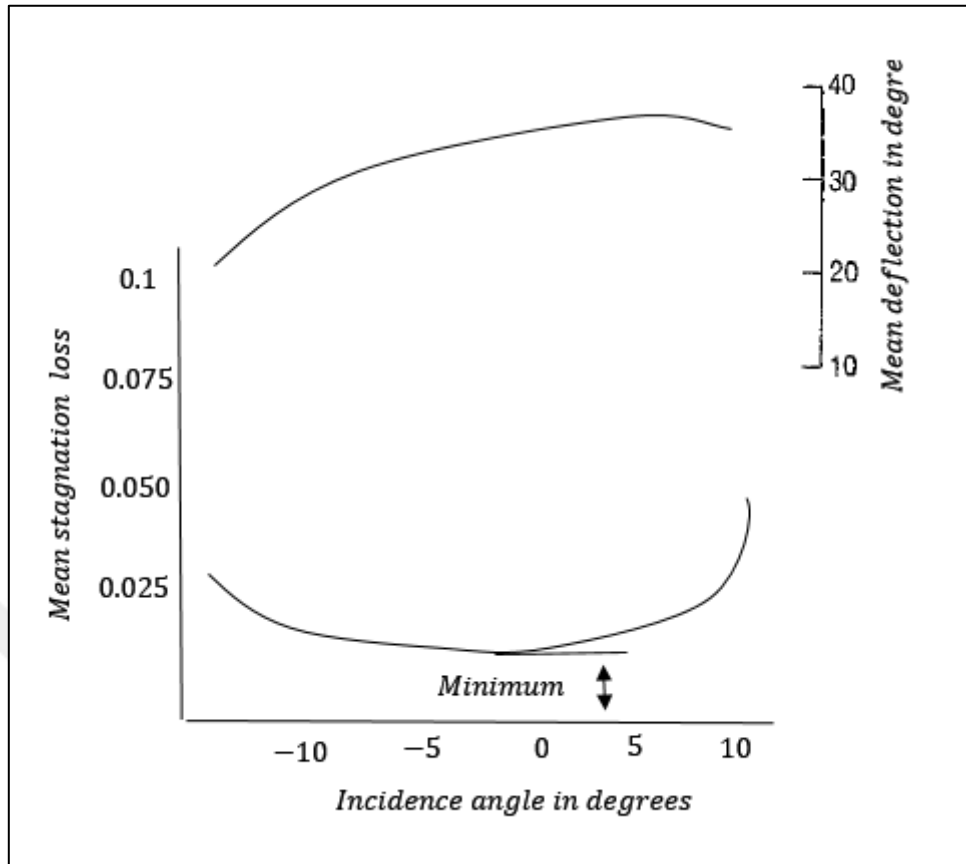


Figure 3.13. Mean deflection and mean stagnation pressure loss for a cascade of the fixed geometrical form [2]

Incidence angle was taken as 0 in the APMC program. For the deviation angle calculations, Carter's rule [21] was utilized which is expressed as follows:

$$\delta = \frac{m_c \theta}{\sqrt{\frac{c}{s}}} \quad (3.50)$$

Where m_c is expressed as follows:

$$m_c = 0.23 \left(\frac{2a}{c}\right)^2 + 0.1 \left(\frac{\beta_2}{50}\right) \quad (3.51)$$

a is the distance of the point of maximum camber from the leading edge of the blade. For circular arc cambers, it is taken as half of c .

In order to complete the construction of the aerofoil, the remaining parameters are expressed as follows:

$$\delta = \beta_2 - \beta_2' \quad (3.52)$$

$$\theta = \beta_1' - \beta_2' \quad (3.53)$$

$$\xi = \beta_1' - \theta \quad (3.54)$$

It should be reminded that β and α are interchangeable, where the selection depends on the calculations which are performed on the rotor or stator.

3.2.10. Work and Flow Coefficient

The work coefficient of a stage is expressed in terms of stagnation enthalpy change and tangential velocity as follows.

$$\psi = \frac{\Delta h_0}{U^2} \quad (3.55)$$

Typical values of the work coefficient (Stage loading) are between 0.3 and 0.5 [5].

Flow coefficient is the ratio of axial velocity to tangential velocity and expressed as follows:

$$\phi = \frac{c_a}{U} \quad (3.56)$$

The value of the flow coefficient varies between 0.3 and 0.9 [5], the trend is to use lower values. The general value of 0.5 is advised by Cumpsty [19]. This ratio determines the incidence angle. High tangential speed results in a lower flow coefficient. Thus incidence angle increases.

3.2.11. Losses and Efficiency in Axial Compressors

The efficiency of the compressor is calculated after annulus size and flow angles were determined. Total losses are the main parameters in efficiency calculations. There are three basic sources of losses that exist in compressor design which are profile losses, end-wall and clearance losses, shock losses. There is an additional source of loss, which is called part span shroud loss and it is valid for fans or the first stage of low-pressure compressors [22]. This type of loss is not considered in the design calculation.

Efficiency calculations are carried on basically examining if the given work input can completely fulfill the final pressure ratio. In order to perform efficiency calculations lift and profile drag coefficients are calculated utilizing cascade test velocity measurements.

From the steady, incompressible flow equation, the static pressure difference across the cascade blades is given as follows:

$$\Delta p = p_2 - p_1 = (p_{02} - 0.5\rho W_2^2) - (p_{01} - 0.5\rho W_1^2) \quad (3.57)$$

The flow is assumed incompressible as change in density is negligible.

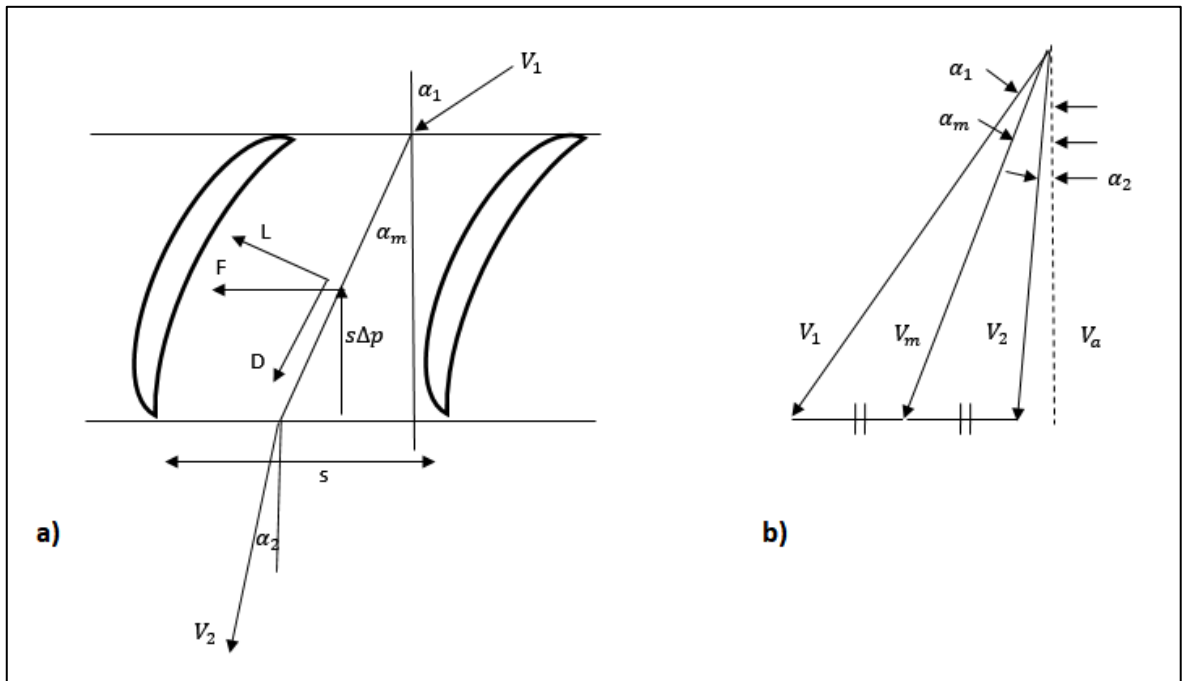


Figure 3.14. Forces acting on the cascade. (a) Cascade forces (b) Vector mean velocity [2]

From the cascade notation Eqn. 3.57 is transformed in terms of axial velocity and the flow angles with the assumption of constant axial velocity [2].

$$\Delta p = 0.5\rho(V_1^2 - V_2^2) - \bar{w} = 0.5\rho V_a^2(\tan \alpha_1^2 - \tan \alpha_2^2) - \bar{w} \quad (3.58)$$

Where \bar{w} stands for mean loss. Forces acting on cascade has two compound which are the axial direction denoted per unit length for each blade $s\Delta p$ and the tangential component due to momentum change F (Figure 3.13).

$$F = s\rho V_a^2(\tan \alpha_1 - \tan \alpha_2) \quad (3.59)$$

Where $V_a(\tan \alpha_1 - \tan \alpha_2)$ is the tangential velocity change.

Utilizing from the velocity triangles illustrated in Figure 3.13, vector mean velocity is expressed as follows:

$$V_m = V_a \sec \alpha_m \quad (3.60)$$

Drag and lift coefficients are calculated considering the vector mean velocity:

$$C_{Dp} = \left(\frac{s}{c}\right) \left(\frac{\bar{w}}{0.5\rho V_1^2}\right) \left(\frac{\cos \alpha_m^3}{\cos \alpha_1^2}\right) \quad (3.61)$$

$$C_L = 2 \left(\frac{s}{c}\right) (\tan \alpha_1 - \tan \alpha_2) \cos \alpha_m \quad (3.62)$$

Instead of the profile drag calculations, alternatively, the plot of test data might be utilized from Figure 3.14.

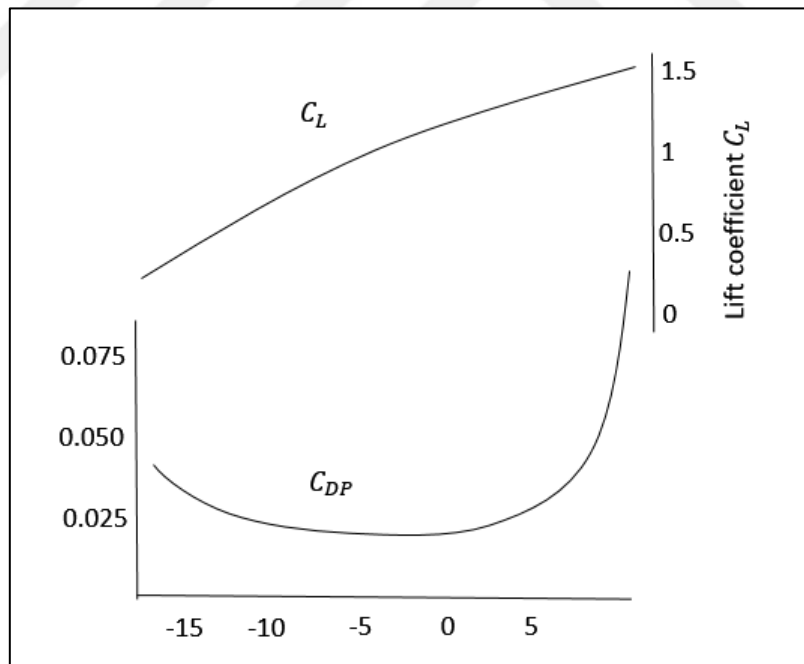


Figure 3.15. Lift & profile drag coefficients for a cascade of the fixed geometrical form [2]

There are additional drag sources, which are caused by secondary losses, and they are expressed as follows:

$$C_{DS} = 0.018C_L^2 \quad (3.63)$$

End wall drag coefficient is expressed as follows:

$$C_{DA} = 0.02 \left(\frac{s}{h} \right) \quad (3.64)$$

Overall drag factor in conjunction with all the above components is expressed as follows:

$$C_D = C_{Dp} + C_{DA} + C_{DS} \quad (3.65)$$

With incorporating shock loss factor \bar{w}_{shock} , therefore total loss factor “w” (It also equals to mean loss divided by inlet dynamic head) can be calculated as follows,

$$w = \left(\frac{\bar{w}}{0.5\rho V_1^2} \right) = C_D \left(\frac{c}{s} \right) \left(\frac{\cos \alpha_1^2}{\cos \alpha_m^3} \right) + \bar{w}_{shock} \quad (3.66)$$

On the other hand, the theoretical pressure rise is given by:

$$\left(\frac{\Delta p_{th}}{0.5\rho V_1^2} \right) = 1 - \frac{\cos \alpha_1^2}{\cos \alpha_2^3} \quad (3.67)$$

The efficiency of blade row therefore given by:

$$n_b = 1 - \frac{\frac{\bar{w}}{0.5\rho V_1^2}}{\frac{\Delta p_{th}}{0.5\rho V_1^2}} \quad (3.68)$$

Stage efficiency n_b can be calculated by the following expression:

$$n_S = \Lambda n_{b,rotor} + (1 - \Lambda) n_{b,stator} \quad (3.69)$$

It should be noted that the above expressions use cascade notation. For rotor calculations relative; for stator calculations, absolute velocities and angles should be taken into account.

Shock waves are known as a type of disturbance, which travels through a medium faster than the speed of sound that belongs to that medium. There are basically two types of shock waveforms that arise across blade rows which are normal shock and oblique shock as illustrated in Figure 3.16. Both occur above Mach 1. Normal shock wave propagates normal to the flow direction. The direction of flow does not change and the flow is always subsonic going through downstream. However oblique shock waves propagate with an angle to the flow direction. Subsonic or supersonic waves might be expected to go through downstream.

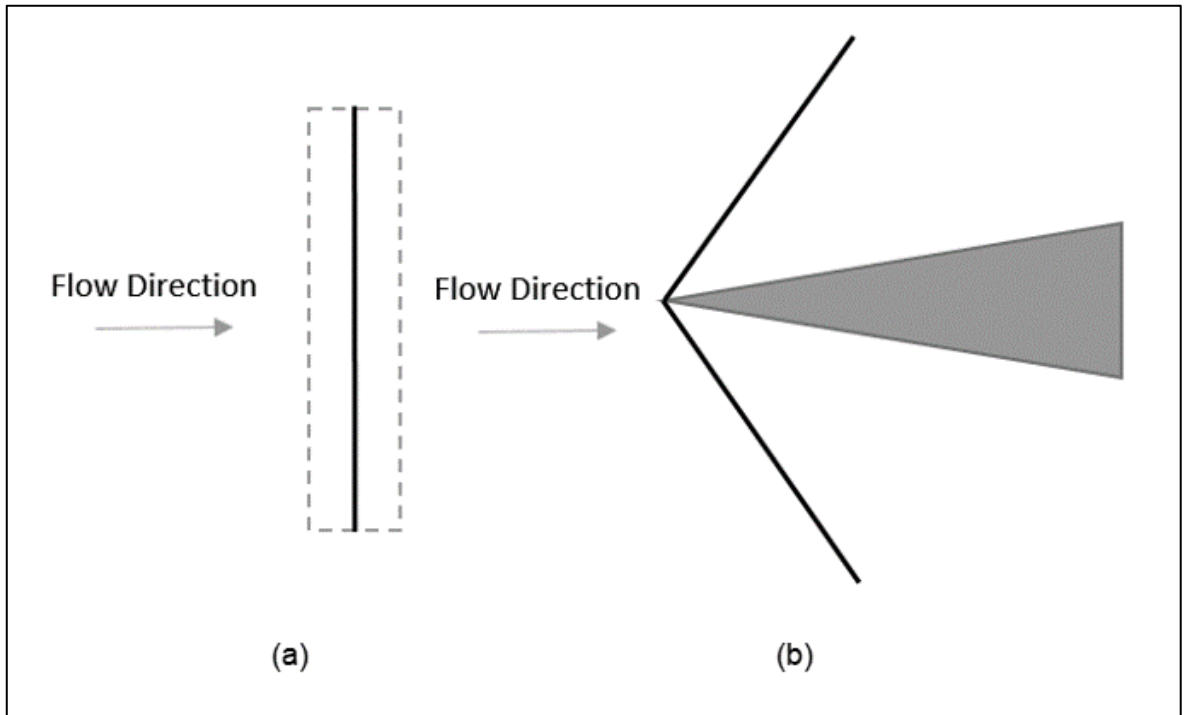


Figure 3.16. Basic wave types. (a) The normal shock wave, (b) Oblique shock wave

According to the Miller et al. [13] calculation method, a shock wave might be approximated as a straight line from one of the leading edge to the adjacent blade suction surface by keeping perpendicularity to mid-channel streamline as illustrated in figure 3.16. Stagnation pressure drop is calculated with a loss of normal shock by an average Mach number which is denoted as M_1 .

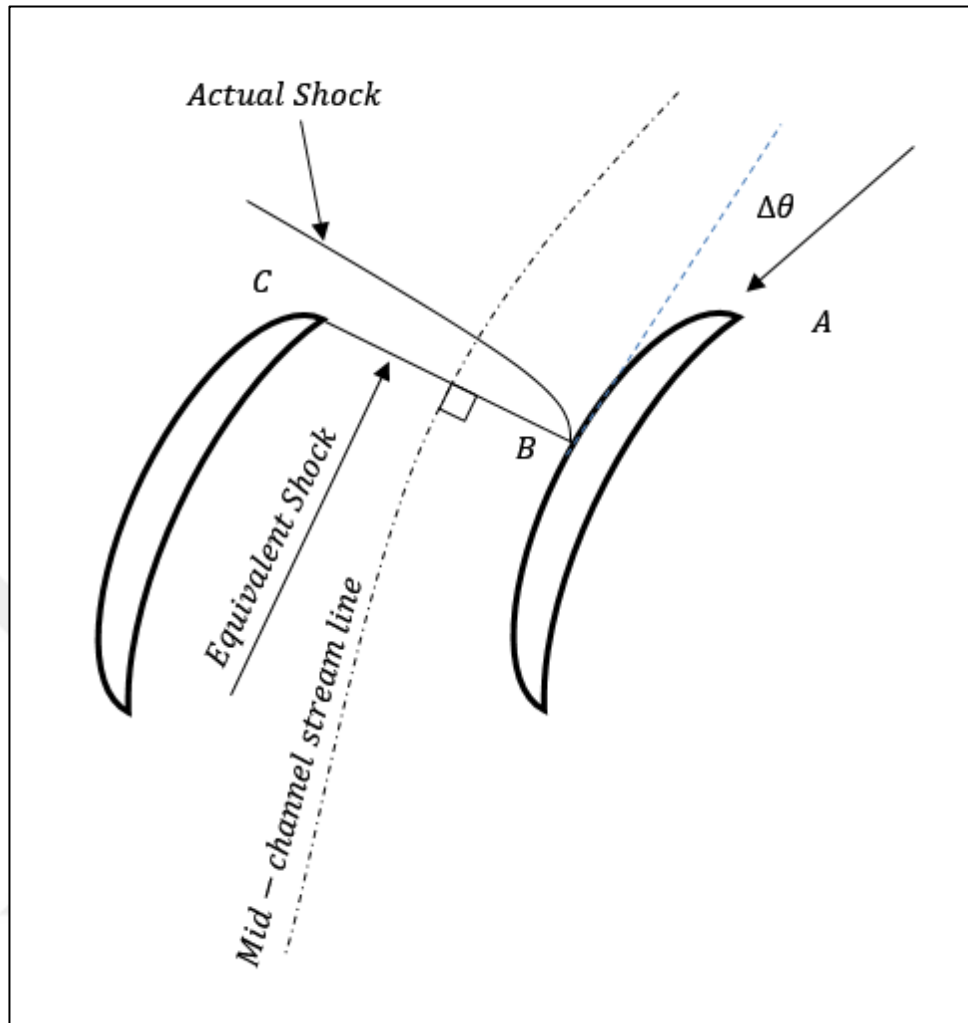


Figure 3.17. Shock loss model of Miller et al. [13]

For the inlet Mach number which is below 1, losses are approximated from experimental data [4]. Thus shock loss coefficient is given by following equation if $0.82 < Mach_{1,rel} < 1.0$:

$$\bar{w}_{shock} = 0.035(Mach_{1,rel} - 0.82) \quad (3.70)$$

Supersonic turning angle is given by the half of the summing inlet and outlet angle:

$$\Delta\theta = \theta_B - \theta_A = 0.5(\alpha_1 - \alpha_2) \quad (3.71)$$

θ_A turning angle is calculated as follows:

$$\theta_A = \sqrt{\frac{\gamma+1}{\gamma-1}} \cos^{-1} \left(\sqrt{\frac{\gamma+1}{2+(\gamma-1)M_A^2}} \right) - \cos^{-1} \left(\frac{1}{M_A} \right) \quad (3.72)$$

In equation 3.72, M_A stands for the relative Mach number for the blade and absolute Mach number for the vane. After θ_A has been calculated, θ_B can be calculated from equation 3.71. Calculation of M_B is an iterative process that is carried on equation 3.73.

$$\theta_B = \sqrt{\frac{\gamma+1}{\gamma-1}} \cos^{-1} \left(\sqrt{\frac{\gamma+1}{2+(\gamma-1)M_B^2}} \right) - \cos^{-1} \left(\frac{1}{M_B} \right) \quad (3.73)$$

Thus θ_B is already known from equation 3.71. An iterative process is carried on via the APMC tool, yields the correct M_B value for the known θ_B .

With the known M_A and M_B the average Mach number is calculated as follows:

$$M_1 = 0.5(M_A + M_B) \quad (3.74)$$

Shock loss coefficient is expressed as follows:

$$\bar{W}_{shock} = \frac{P_{02} - P_{01}}{P_{0A} - P_A} = \frac{1 - \left(\frac{P_{02}}{P_1}\right) \left(\frac{P_1}{P_{01}}\right)}{1 - \left(\frac{P_A}{P_{0A}}\right)} \quad (3.75)$$

Where P_{01} stands for upstream stagnation pressure and P_{02} stands for downstream stagnation pressure of normal shock wave. Utilizing gas dynamics relations, for an adiabatic normal shock:

$$\frac{P_{02}}{P_1} = \frac{\left[\frac{\gamma+1}{2} M_1^2 \right]^{\frac{\gamma}{\gamma-1}}}{\left[\frac{2\gamma M_1^2 - (\gamma-1)}{\gamma+1} \right]^{\frac{1}{\gamma-1}}} \quad (3.76)$$

For isentropic flow, shock loss formulations are as follows:

$$\frac{P_{02}}{P_1} = \left(1 + \frac{\gamma-1}{2} M_1^2 \right)^{\frac{\gamma}{\gamma-1}} \quad (3.77)$$

$$\frac{P_A}{P_{0A}} = \left(1 + \frac{\gamma-1}{2} M_A^2 \right)^{\frac{\gamma}{\gamma-1}} \quad (3.78)$$

3.2.12. Initial Sizing and Shaft Speed Calculations for a Stage

Initial annulus sizes should be calculated in order to have a good start point for optimization. The calculation procedure is detailed as follows:

Due to continuity, the mass flow rate is given by:

$$\dot{m} = \rho_1 A_1 C_{a1} = \rho_1 \pi r_{1,tip}^2 \left[1 - \left(\frac{r_{1,hub}}{r_{1,tip}} \right)^2 \right] C_{a1} \quad (3.79)$$

Due to isentropic compression, ρ_1 is calculated by the following expressions:

$$\rho_1 = \frac{P_1}{R T_1} \quad (3.80)$$

$$T_1 = T_{01} - \frac{C_1^2}{2c_p} \quad (3.81)$$

Where T_{01} stands for the stagnation temperature of the inlet which is taken as ambient temperature.

$$P_1 = P_{01} \left(\frac{T_1}{T_{01}} \right)^{\frac{\gamma}{\gamma-1}} \quad (3.82)$$

Where P_{01} stands for the stagnation pressure of inlet which is taken as ambient atmospheric pressure.

The tip speed of the blade is usually taken as 350 m/sec which does not result in excessive stress and shock loss [2]. Therefore shaft speed is given by:

$$N = \frac{U_{1,tip}}{2\pi r_{1,tip}} \quad (3.83)$$

Hub to tip ratio of 0.5 would be a good start for calculations. After introducing inlet sizes and speed into the APMC tool, a manual trial-error or optimization process will give the optimum annulus shape.

3.3. PRELIMINARY MECHANICAL DESIGN OF AXIAL COMPRESSOR

3.3.1. Centrifugal Stress at Blade Root Section

The major mechanical constraint is centrifugal stress, which is caused by the centrifugal effect on the rotor blade. The greatest stress at the rotor blade occurs at the root section.

$$U_{tip} = 2\pi N r_{tip} \quad (3.84)$$

$$\sigma_{root} = \frac{\rho_{blade}}{2} U_{tip}^2 \left[1 - \left(\frac{r_{hub}}{r_{tip}} \right)^2 \right] \quad (3.85)$$

Equation 3.85 can be written in another form in terms of angular velocity which is given by:

$$\sigma_{root} = \frac{\rho_{blade}}{2} N^2 [r_{tip}^2 - r_{hub}^2] \quad (3.86)$$

Equation 3.85 and 3.86 assume that the blade is constituted by a constant cross-section. Blades are usually has a taper through span and the tip area is smaller. Therefore the stress is smaller than the calculation which is done with equation 3.85 and 3.86. Small hub to tip ratio $\left(\frac{r_r}{r_t}\right)$ results in high centrifugal stress at the blade root section. In other words, the combination which has a high blade tip radius and low hub radius results in high centrifugal root stress. Due to the stress concentration factor at the root section, actual stress may deviate from analytical solutions.

Gas bending stress occurs at the root section due to tangential momentum change. In compressor design, gas bending stress occurs also due to pressure differential between the up and downstream flow. However, for the preliminary design concept, it can be omitted [2]. Gas bending stress in the tangential direction is then given by:

$$\sigma_{gb} = \frac{\dot{m} \Delta C_w}{NB} \frac{h}{2 I_{tangential}} y \quad (3.87)$$

Where y stands for the distance that is from the neutral axis to the point where the bending stress will be examined. For instance, if a suction side stress is examined from the utmost point of suction side to the neutral axis, which is the distance imposed into y . In expression

3.87, $I_{\text{tangential}}$ stands for the area moment of inertia of the root section about the axis which is almost perpendicular to tangential direction.

Centrifugal untwist stress occurs under the effect of centrifugal load thus blade tends to untwist itself. The most efficient way of calculating this stress is FEA.

Finally, blade tilt stress occurs due to the bending effect of mismatch between the blade center of gravity and the blade neutral point of the root section. Tilt stress is mostly used for offsetting gas bending stress to desired sides, suction or pressure, leading edge or trailing edge.

In the preliminary design step, FEA might be used so as to encompass stress components which are centrifugal, untwist, blade tilt stresses. Gas bending stress will not be incorporated into the stress assessment because it is generally used for high cycle fatigue assessment that is not in the concept of this thesis.

3.3.2. Blade Resonance

Another item, which should be assessed in terms of structural integrity, is resonance. Blades are assumed as cantilever beams. The natural period of a cantilever beam is the travel duration of tip point when it oscillates. If a small amount of exciter reacts with the blade as the same period of oscillating thus deflection goes infinity if there is no adequate damping factor. This effect causes the blade sudden fracture. 1 over the natural period is called natural frequency. The compressor system should not include the number of exciters colliding with any natural frequency of blade.

Natural frequency calculation should be certain and validated by the tests. Modal analysis is one of the ways to determine blade natural frequencies. 3 basic modal shapes which are flap wise or flexural, torsional and stripe can be determined.

For preliminary design purposes, 1st flexural natural frequency was taken into account in this thesis.

3.4. OPTIMIZATION PROCESS

The compressor optimization process is a complex task due to the multi-objective nature of the problem and several disciplines should be encompassed simultaneously. Although the APMC tool permits conducting the traditional trial-and-error method this is not the best way so as to find optimum geometric combinations of the input parameters with respect to both aerodynamic and structural output parameters.

3.4.1. Design of Experiment

The design of experiment is generally starting point for all types of optimization processes. DOE approach provides to determine the general behaviour of the examined objective function. The importance of input variables that contribute to the change in output parameters is quantified.

Full factorial is one of the methods used in the DOE study. The full factorial method considers all of the information about the influence of each variable at each interaction. The number of the experiment is given by:

$$\text{Number of Experiment} = [\text{Number of Levels}]^{\text{Number of Variables}} \quad (3.88)$$

Considering 10 parameters which have 3 levels for each, yields $3^{10} = 59049$ experiments. Performing these experiments take too much time. In order to reduce the number of experiments, one of the most commonly used methods is Central Composite design (CCD) [23].

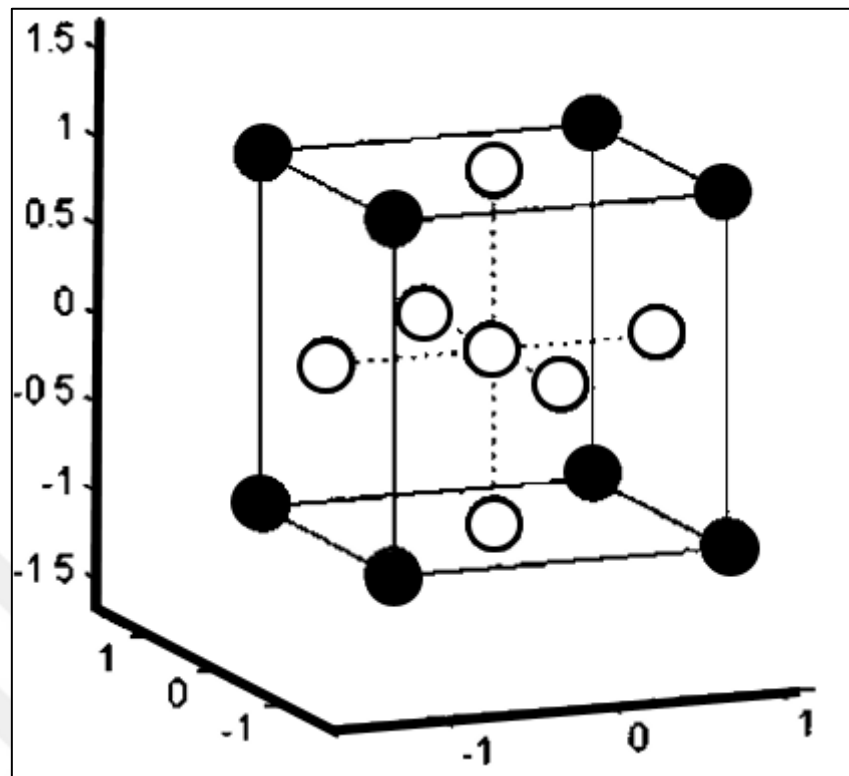


Figure 3.18. Face centred CCD design space [24]

In ACMC Face Centred CCD has been used. The number of levels is given as 5. The levels are expressed by $[-\alpha, -1, 0, +1, +\alpha]$, where $\alpha = 1$, therefore, it is transformed into 3 levels design. The design space of Face Centred CCD is illustrated in Figure 3.18. The filled circles denote the physical limits of the parameter (At the corners), empty circles denote physical extremes. In Face Centred type DOE scheme, filled and empty circles stay in the same plane.

Table 3.1. The number of experiment in the Face Centred CCD method [24]

| Number of Parameters, NP | Factorial, f | Number of Center Point, NCP | Number of Axis | Number of Diagonal | Number of Experiment |
|--------------------------|--------------|-----------------------------|----------------|--------------------|----------------------|
| 1 | 0 | 1 | 2 | 2 | 5 |
| 2 | 0 | 1 | 4 | 4 | 9 |
| 3 | 0 | 1 | 6 | 8 | 15 |
| 4 | 0 | 1 | 8 | 16 | 25 |
| 5 | 1 | 1 | 10 | 16 | 27 |
| 6 | 1 | 1 | 12 | 32 | 45 |
| 7 | 1 | 1 | 14 | 64 | 79 |
| 8 | 2 | 1 | 16 | 64 | 81 |
| 9 | 2 | 1 | 18 | 128 | 147 |
| 10 | 3 | 1 | 20 | 128 | 149 |
| 11 | 4 | 1 | 22 | 128 | 151 |
| 12 | 4 | 1 | 24 | 256 | 281 |
| 13 | 5 | 1 | 26 | 256 | 283 |
| 14 | 6 | 1 | 28 | 256 | 285 |
| 15 | 7 | 1 | 30 | 256 | 287 |
| 16 | 8 | 1 | 32 | 256 | 289 |
| 17 | 9 | 1 | 34 | 256 | 291 |
| 18 | 9 | 1 | 36 | 512 | 549 |
| 19 | 10 | 1 | 38 | 512 | 551 |
| 20 | 11 | 1 | 40 | 512 | 553 |

The number of the experiment is denoted by NE and it is given by:

$$NE = NCP + 2NP + 2^{(NP-f)} \quad (3.89)$$

If we recalculate for 10 parameters with 3 levels for each, equation 3.89 yields 149 experiments to be investigated. Compared to full factorial design, Face Centred CCD gives an affordable number of experiments.

3.4.2. Polynomial Response Surface Method

The polynomial response surface method builds a polynomial where a correlation is maintained between input and output parameters. Second-order polynomial response surface is widely used because of flexibility and the expression is given by for the N variables [23]:

$$y = \beta_0 + \sum_{i=1}^N \beta_i x_i + \sum_{i=1}^N \beta_i x_i^2 + \sum \sum_{i \neq j}^N \beta_{ij} x_i x_j + \epsilon \quad (3.90)$$

Where x_i stands for the input parameters, β_0 stands for the mean value of the regression model, β_i stands for the linear coefficients, β_{ii} stands for the second-order coefficients, β_{ij} stands for the interaction coefficients, ϵ stands for the total error which is the difference between the actual and the predicted response. The least-squares regression method is applied and the coefficients are determined. A response surface is created for each output parameter.

3.4.3. Multi Objective Genetic Algorithm Optimization

Due to the nature of compressor design, there are numerous input and output parameters that exist and there may be several optimum points. Genetic algorithm is one of the most widely used techniques for finding global optimum thus preferred in turbomachinery optimization [25]. The genetic algorithm procedure basically starts with the selection of couples from the population set. Then the parameters are converted to binary system and appended consecutively to build a long binary string for each member of the couples. Two parents (A couple) are selected, some of the bits are interchanged among parents to build 2 new children (Crossover). 1 percent of a long binary string of children are changed arbitrarily (Mutation). After generating children, the problem is evaluated for the objective function and better child or parent is kept, the rest of them are destroyed until the criteria are satisfied.

Design variables (Input parameters) are written in a vector form as follows:

$$\vec{X} = \begin{bmatrix} r_{1,tip} \\ r_{2,tip} \\ r_{3,tip} \\ r_{4,tip} \\ r_{1,hub} \\ r_{2,hub} \\ r_{3,hub} \\ r_{4,hub} \\ \alpha_{4,mean} \\ \beta_{2,mean} \end{bmatrix} \quad (3.91)$$

Objective functions are expressed for each output parameter as following example formulations:

$$f \begin{pmatrix} f_1(\vec{X}) \\ \vdots \\ f_n(\vec{X}) \end{pmatrix} = \begin{cases} DF_{rotor,tip} \\ \vdots \\ \sigma_{root} \end{cases} \quad (3.92)$$

After objectives are set as expressed in equation 3.92, pseudo-objective function “ \vec{F} ”, which contains weight factor “ z ”, is shown in the following expression:

$$\vec{F} = \sum_{i=1}^n z_i f_i(\vec{X}) \quad (3.93)$$

Weight factor varies between 0 and 1; the summation of all should be 1. While the important objectives have the values close to 1, values for less important objectives should be close to 0. The importance of the objective depends on the experience of designers. The pseudo-objective function is minimized or maximized but sometimes some of the objectives are set to be maximized and some of them minimized in the same problem. In those kinds of situations if the parameter is reversed as “1/parameter” then the objective function is transformed into the form of entire maximizing or minimizing-problem.

4. ACMC TOOL CALCULATION PROCEDURE

ACMC is a Spreadsheet-based tool, which basically calculates, compression ratio, stage efficiency, diffusion factors, de Haller numbers, flow coefficients, work coefficients, pitch to cord ratio, aspect ratio, Mach numbers, air and corresponding blade angles, centrifugal stress, losses for the given annulus sizes, mass flow rate and the shaft speed utilizing basic thermodynamics and empirical correlations as previously explained. The block diagram of the design procedure is given in Figure 4.1.

The design begins with collecting design parameters and customer requirements such as size limits and related constraints. Upper and lower boundaries are determined depending on user experiences. Too wide boundaries may increase the chance to find optimum points but there may be no-solution points, which are encountered. Those points cannot be used in optimization. The trial and error method can be useful while assessing lower and upper boundaries via the ACMC tool so as to prevent encountering no-solution points.

After determining boundaries, arbitrary input values, which are between upper and lower boundaries, are introduced into ACMC in order to determine the baseline design point. It is expected that the efficiency and compression ratio of the baseline design point is low. According to the number of input parameters and selected DOE scheme, DOE and related design points (Design space) are generated via Ansys Workbench. Design points are introduced into ACMC and corresponding output parameters are calculated for each. A response surface is created for each output parameter in order to provide the best fit functions to interpolate the space. Criteria are introduced as objectives and multi-objective genetic algorithm optimization is conducted. After optimization, candidate design points are verified with ACMC to assess if interpolated values are close enough to exact values (Actual solve). Mechanical analyses are carried on Ansys Mechanical corresponding to selected material. The final step is to perform 3D CFD analysis and results are compared with the analytical solution.

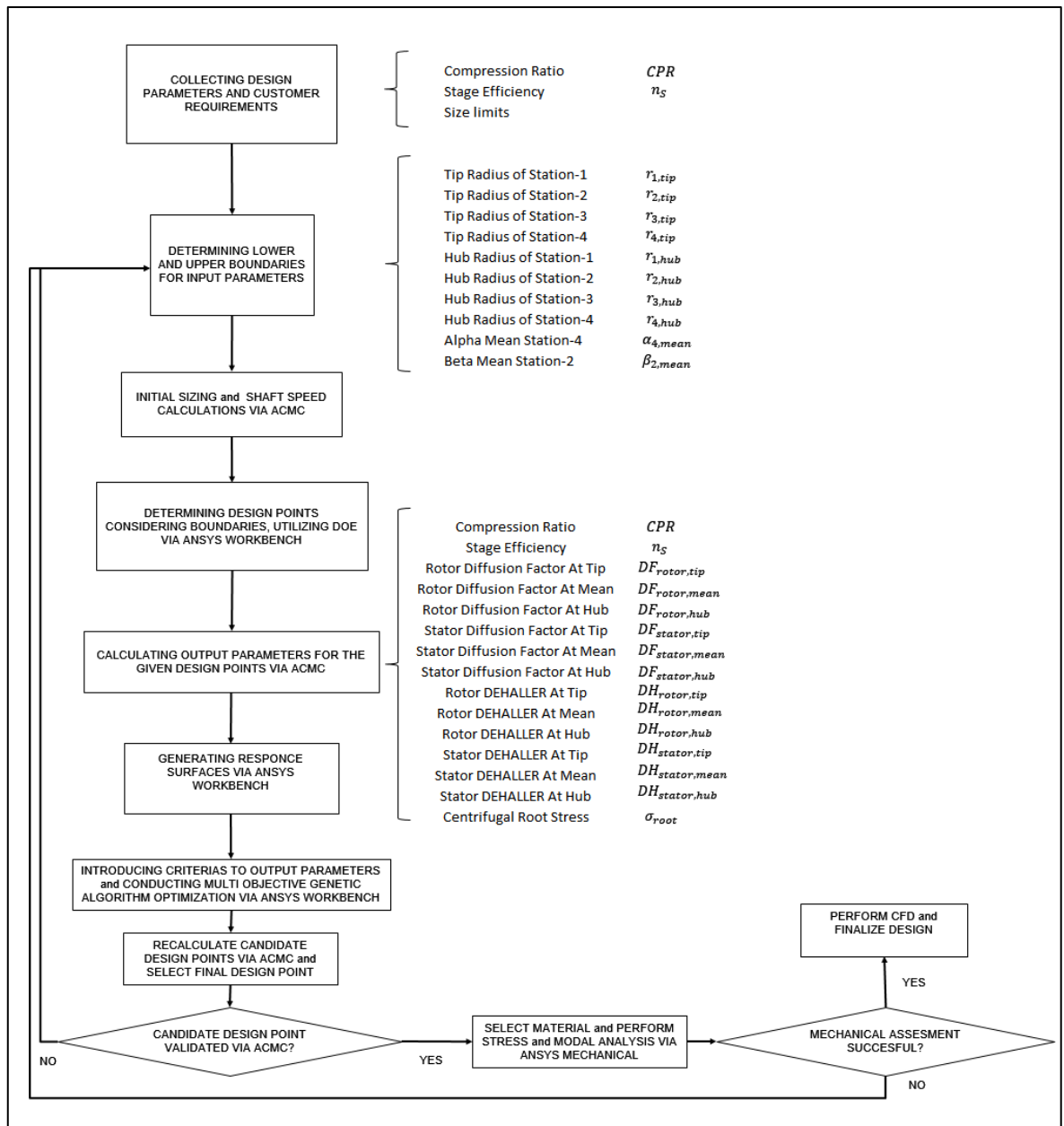


Figure 4.1. Block diagram for ACMC design procedure

4.1. FORMULATIONS

There are 4 calculation stations in the tool as illustrated in Figure 4.2. Stations 1 and 2 denote rotor inlet and outlet locations respectively, Stations 3 and 4 denote stator vane inlet and outlet locations. Station 1 calculations are detailed as follows:

Axial velocity was not assumed to be constant through the compressor. Calculation of correct axial velocity was based on finding both densities from continuity and equation of state then performing iteration until both densities are equal. Axial velocity, which makes both densities equal, is the correct axial velocity. After determining initial annulus sizes and shaft speed from equation 3.79 through 3.83, an arbitrary value is assigned to ρ_1 then inlet axial velocity C_{a1} is calculated as follows:

$$C_{a1} = \frac{\dot{m}}{\rho_1 A_1} \quad (4.1)$$

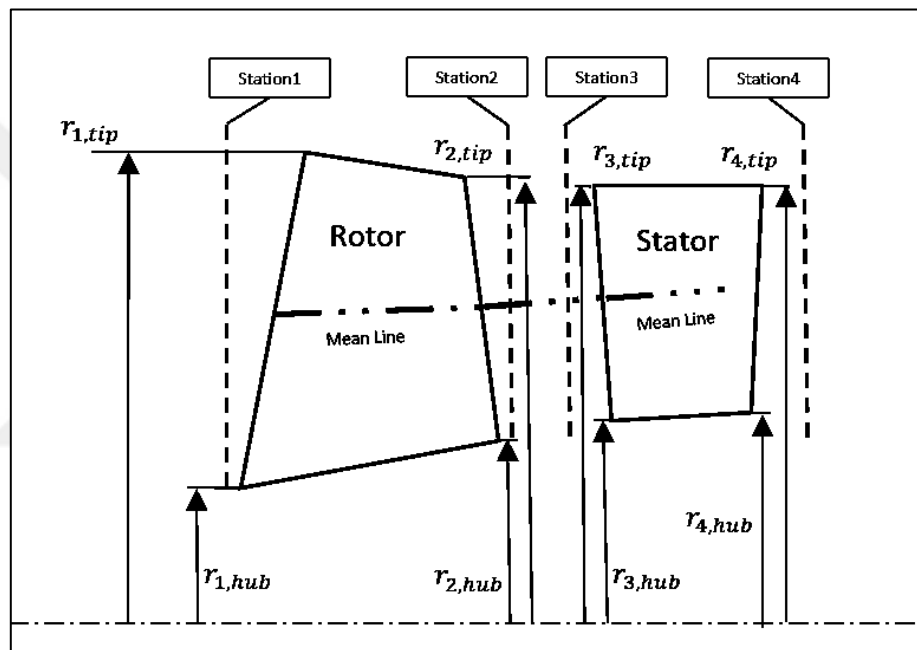


Figure 4.2. ACMC tool layout

The static temperature at the inlet is calculated for inlet absolute velocity C_1 ,

$$C_1 = \frac{C_{a1}}{\cos \alpha_1} \quad (4.2)$$

$$T_1 = T_{01} - \frac{C_1^2}{2c_p} \quad (4.3)$$

Static pressure P_1 is calculated at a calculated temperature as follows:

$$P_1 = P_{01} \left(\frac{T_1}{T_{01}} \right)^{\frac{\gamma}{\gamma-1}} \quad (4.4)$$

Then from the equation of state, ρ_1 is calculated again and iterated until initial ρ_1 and final ρ_1 are both equal to each other. Iterative solutions are conducted utilizing the Solver add-in program in Microsoft Excel.

$$\rho_1 = \frac{P_1}{RT_1} \quad (4.5)$$

At Station 2 following calculation steps are followed:

Assign an arbitrary value to ρ_2 then calculate an axial velocity C_{a2} as follows:

$$C_{a2} = \frac{\dot{m}}{\rho_2 A_1} \quad (4.6)$$

Assign an arbitrary value to β_2 then calculate an inlet axial velocity C_{a2} as follows:

$$W_2 = \frac{C_{a2}}{\cos \beta_2} \quad (4.7)$$

α_2 is calculated from the velocity triangles as follows:

$$\alpha_2 = \tan^{-1} \left(\frac{U_2 - W_2 \sin \beta_2}{C_{a2}} \right) \quad (4.8)$$

$$C_2 = \frac{C_{a2}}{\cos \alpha_2} \quad (4.9)$$

$$C_{w1} = C_1 \sin \alpha_1 \quad (4.10)$$

$$C_{w2} = C_2 \sin \alpha_2 \quad (4.11)$$

$$T_{02} = T_{01} + \frac{\lambda(U_2 C_{w2} - U_1 C_{w1})}{c_p} \quad (4.12)$$

$$T_2 = T_{02} - \frac{C_2^2}{2c_p} \quad (4.13)$$

$$P_{02,REL} = P_{01,REL} - w(P_{01,REL} - P_1) \quad (4.14)$$

Where “w” stands for total loss factor (Refer to Eqn. 3.66 for detailed explanation). Δs stands for entropy change, which is expressed as follows:

$$\Delta s = -R \ln \left(\frac{P_{02,REL}}{P_{01,REL}} \right) \quad (4.15)$$

$$P_{02} = P_{01} \frac{c_p \ln\left(\frac{T_{02}}{T_{01}}\right) - \frac{\Delta s}{R}}{R} \quad (4.16)$$

$$P_2 = P_{02} \left(\frac{T_2}{T_{02}}\right)^{\frac{\gamma}{\gamma-1}} \quad (4.17)$$

Then from the equation of state, ρ_2 is calculated again and iterated until both densities are equal

$$\rho_2 = \frac{P_2}{RT_2} \quad (4.18)$$

For Station 3 calculations assume $\alpha_3 = \alpha_2$. Assign an arbitrary value to ρ_3 then calculate an axial velocity C_{a3} as follows:

$$C_{a3} = \frac{\dot{m}}{\rho_3 A_3} \quad (4.19)$$

$$C_3 = \frac{C_{a3}}{\cos \alpha_3} \quad (4.20)$$

Between Station 2 and 3, the control volume is assumed to be adiabatic and no kinetic energy addition occurs. Therefore the total pressure and temperature change is constant $P_{03} = P_{02}$, $T_{03} = T_{02}$.

$$T_3 = T_{03} - \frac{C_3^2}{2c_p} \quad (4.21)$$

$$P_3 = P_{03} \left(\frac{T_3}{T_{03}}\right)^{\frac{\gamma}{\gamma-1}} \quad (4.22)$$

Then from the equation of state, ρ_3 is calculated again and iterated until both densities are equal.

$$\rho_3 = \frac{P_3}{RT_3} \quad (4.23)$$

For Station 4 assign an arbitrary value to ρ_4 then calculate an outlet axial velocity C_{a4} as follows:

$$C_{a4} = \frac{\dot{m}}{\rho_4 A_4} \quad (4.24)$$

Assign an arbitrary value to α_4 then calculate an absolute velocity C_4 as follows:

$$C_4 = \frac{C_{a4}}{\cos \alpha_4} \quad (4.25)$$

Between Station 3 and 4, the control volume is assumed to be adiabatic and there exists no kinetic energy addition, therefore, the total temperature change is constant $T_{04} = T_{03}$.

$$T_4 = T_{04} - \frac{C_4^2}{2c_p} \quad (4.26)$$

$$P_{04} = P_{03} - w(P_{03} - P_3) \quad (4.27)$$

Where “w” stands for total loss factor (Refer to Eqn. 3.66 for detailed explanation).

$$Ma_4 = \frac{C_4}{\sqrt{\gamma RT_4}} \quad (4.28)$$

$$P_4 = \frac{P_{04}}{(1+0.5(\gamma-1)Ma_4^2)^{\frac{\gamma}{\gamma-1}}} \quad (4.29)$$

Then from the equation of state, ρ_4 is calculated again and iterated until both densities are equals to each other.

$$\rho_4 = \frac{P_4}{RT_4} \quad (4.30)$$

Free vortex condition $C_w r = Constant$. Related air angles from hub to tip are calculated as follows:

$$(C_{w2}r)_{mean} = (C_{w2}r)_{tip} = (C_{w2}r)_{hub} \quad (4.31)$$

$$(\alpha_2)_{tip} = \tan^{-1} \left(\frac{C_{w2}}{C_{a2}} \right)_{tip} \quad (4.32)$$

$$(\alpha_2)_{hub} = \tan^{-1} \left(\frac{C_{w2}}{C_{a2}} \right)_{hub} \quad (4.33)$$

$$(\beta_2)_{tip} = \tan^{-1} \left(\frac{U_2 - C_{w2}}{C_{a2}} \right)_{tip} \quad (4.34)$$

$$(\beta_2)_{mean} = \tan^{-1} \left(\frac{U_2 - C_{w2}}{C_{a2}} \right)_{mean} \quad (4.35)$$

$$(\beta_2)_{hub} = \tan^{-1} \left(\frac{U_2 - C_{w2}}{C_{a2}} \right)_{hub} \quad (4.36)$$

Speed of sound and Mach number is calculated to prevent excessive shock loss build-up:

$$c = \sqrt{\gamma RT_2} \quad (4.37)$$

$$(Ma_{2REL})_{hub,mean,tip} = \frac{(W_2)_{hub,mean,tip}}{c} \quad (4.38)$$

$$(Ma_{2ABS})_{hub,mean,tip} = \frac{(C_2)_{hub,mean,tip}}{c} \quad (4.39)$$

The compression ratio is calculated as follows:

$$CPR = \frac{P_{02}}{P_{01}} \quad (4.40)$$

Basic calculation steps were given with the above equations. All the required design parameters were given in Chapter 3 in more detail.

5. COMPARING ACMC TOOL AND CFD RESULTS

As mentioned in previous chapters, preliminary design encompasses many design parameters that should be kept in predefined ranges simultaneously. The traditional trial-error method, of course, would converge the design to an allowable parameter set however it would not be the optimum design point. So as to validate the method, which is mentioned in this thesis, 20kg/sec axial compressor has been designed and optimized. "0.2242m" radius value is introduced as a size limit of customer requirement, which will not be exceeded.

In order to collect good start point data for optimization, initial values were calculated from the equations, which are given in section 3.2.12. Relative Mach number of the blade tip is 1.1715 that is in transonic range. Therefore it is convenient to use DCA blading. Hub to tip ratio of 0.509 was selected for the blade. Inlet hub and tip radii were calculated as 0.1131m and 0.2222m respectively.

After introducing initial values into ACMC, stage calculation begins. Figure 5.1 through Figure 5.4 shows part of the user interface of the ACMC tool. "Sta 1, 2, 3, 4" stands for the calculation stations as illustrated in Figure 4.1 in the previous chapter. Stations 2, 3, 4 radii were set to free but exceeding of 0.2242m was not allowed. "Sta 2,3" hub and tip radii are set equal in order to prevent sudden expansion in the narrow region and reducing the number of input parameters. The manual trial-error method was used so as to introduce an appropriate set of parameters into ACMC. After finding radii, Alpha of Station 4 has been set to 10° and Beta of Station 2 has been set to 52° . Figure 5.5 shows the post-processing data. Each should be in the specific ranges which are aforementioned in Chapter 3. As a reminder, the Diffusion Factor for the tip section should not be exceeded by 0.4, for the mean line 0.43 and for the hub section 0.48. De Haller number should not be under 0.69 (Increasing blade loading purpose). The equivalent Diffusion Factor should be less than 2 for all sections. The work coefficient should be between 0.3 and 0.5. The flow coefficient should be between 0.3 and 0.9.

Table 5.1 shows the compression ratio and efficiency of the initial design. The optimization goal is to set the efficiency and compression ratio as high as possible.

| | | Sta 1 | Sta 2 | Sta 3 | Sta 4 |
|-------------------|------|-------------|-------------|-------------|-------------|
| RADIUS | Tip | 0.2222 | 0.2100 | 0.2100 | 0.2100 |
| | Mean | 0.1677 | 0.1650 | 0.1650 | 0.1655 |
| | Hub | 0.1131 | 0.1200 | 0.1200 | 0.1210 |
| AREA | | 0.1149 | 0.0933 | 0.0933 | 0.0925 |
| ALPHA (Air) | Tip | 0.0000 | 15.8027 | 15.8027 | 7.9113 |
| | Mean | 0.0000 | 19.8095 | 19.8095 | 10.0000 |
| | Hub | 0.0000 | 26.3487 | 26.3487 | 13.5593 |
| ALPHA (Blade) | Tip | | | 15.8027 | 4.7844 |
| | Mean | | | 19.8095 | 6.6208 |
| | Hub | | | 26.3487 | 9.8395 |
| BETA (Air) | Tip | 65.9804 | 61.0053 | | |
| | Mean | 59.4322 | 52.0000 | | |
| | Hub | 48.7974 | 34.8977 | | |
| BETA (Blade) | Tip | 65.9804 | 58.6580 | | |
| | Mean | 59.4322 | 49.2565 | | |
| | Hub | 48.7974 | 31.2830 | | |
| Deflection | Tip | 15.8027 | | 7.8914 | |
| | Mean | 19.8095 | | 9.8095 | |
| | Hub | 26.3487 | | 12.7893 | |
| ABS TOTAL PRESSUE | Tip | 101325.0000 | 116109.6407 | 116109.6407 | 115711.6668 |
| | Mean | 101325.0000 | 117855.5836 | 117855.5836 | 117361.1652 |
| | Hub | 101325.0000 | 119092.0131 | 119092.0131 | 118408.5428 |
| REL TOTAL PRESSUE | Tip | 202611.4147 | 194431.4526 | | |
| | Mean | 152849.6433 | 148884.3067 | | |
| | Hub | 122909.0817 | 120976.4793 | | |
| STATIC PRESSURE | Tip | 86724.8468 | 98437.3720 | 98438.2558 | 99835.1934 |
| | Mean | 86724.8468 | 99143.1925 | 99144.1257 | 101082.0769 |
| | Hub | 86724.8468 | 98378.8085 | 98379.8345 | 101576.2477 |
| ABS TOTAL TEMP | Tip | 288.0000 | 302.9672 | 302.9672 | 302.9672 |
| | Mean | 288.0000 | 302.9672 | 302.9672 | 302.9672 |
| | Hub | 288.0000 | 302.9672 | 302.9672 | 302.9672 |
| REL TOTAL TEMP | Tip | 351.0568 | 344.0171 | | |
| | Mean | 323.8964 | 322.4651 | | |
| | Hub | 304.3369 | 306.0856 | | |
| STATIC TEMP | Tip | 275.4773 | 289.0064 | 289.0072 | 290.4638 |
| | Mean | 275.4773 | 288.3647 | 288.3654 | 290.3193 |
| | Hub | 275.4773 | 286.8710 | 286.8719 | 289.9872 |

Figure 5.1. Stage calculations at ACMC of initial design point, Part-1

| | | | | | |
|--------------------------------|------|----------|----------|----------|----------|
| DENSITY | Tip | 1.0969 | 1.1868 | 1.1868 | 1.1976 |
| | Mean | 1.0969 | 1.1980 | 1.1980 | 1.2132 |
| | Hub | 1.0969 | 1.1949 | 1.1949 | 1.2205 |
| Ca (Axial Velocity) | Tip | 158.6522 | 161.1833 | 161.1790 | 157.0210 |
| | Mean | 158.6522 | 161.1833 | 161.1790 | 157.0210 |
| | Hub | 158.6522 | 161.1833 | 161.1790 | 157.0210 |
| U (Tangential Velocity) | Tip | 356.0116 | 336.4646 | | |
| | Mean | 268.6109 | 264.3650 | | |
| | Hub | 181.2102 | 192.2655 | | |
| Cw (Swirl Velocity) | Tip | 0.0000 | 45.6184 | 45.6172 | 21.8200 |
| | Mean | 0.0000 | 58.0598 | 58.0582 | 27.6870 |
| | Hub | 0.0000 | 79.8322 | 79.8301 | 37.8695 |
| C (Absolute Velocity) | Tip | 158.6522 | 167.5145 | 167.5100 | 158.5298 |
| | Mean | 158.6522 | 171.3213 | 171.3168 | 159.4433 |
| | Hub | 158.6522 | 179.8701 | 179.8653 | 161.5230 |
| W (Relative Velocity) | Tip | 389.7624 | 332.5230 | | |
| | Mean | 311.9653 | 261.8051 | | |
| | Hub | 240.8478 | 196.5230 | | |
| Ma-Rel (Relative Mach) | Tip | 1.1715 | 0.9758 | | |
| | Mean | 0.9377 | 0.7691 | | |
| | Hub | 0.7239 | 0.5788 | | |
| Ma-Abs (Absolute Mach) | Tip | 0.4769 | 0.4916 | 0.4916 | 0.4640 |
| | Mean | 0.4769 | 0.5033 | 0.5033 | 0.4668 |
| | Hub | 0.4769 | 0.5298 | 0.5298 | 0.4732 |
| SPEED OF SOUND | Tip | 332.6963 | 340.7679 | 340.7684 | 341.6261 |
| | Mean | 332.6963 | 340.3894 | 340.3898 | 341.5411 |
| | Hub | 332.6963 | 339.5067 | 339.5072 | 341.3457 |

Figure 5.2. Stage calculations at APMC of initial design point, Part-2

| | | Sta 1 | Sta 2 | Sta 3 | Sta 4 |
|-------------------------|------|----------|--------|----------|--------|
| n- NumOfBLD | | 43 | | 30 | |
| h- BLD Height | | 0.1091 | 0.0900 | 0.0900 | 0.0890 |
| Chord (c) | Tip | 0.0370 | | 0.0330 | |
| | Mean | 0.0370 | | 0.0330 | |
| | Hub | 0.0370 | | 0.0330 | |
| Pitch (s) | Tip | 0.0307 | | 0.0440 | |
| | Mean | 0.0241 | | 0.0347 | |
| | Hub | 0.0175 | | 0.0253 | |
| Camber Angle | Tip | 7.3225 | | 11.0183 | |
| | Mean | 10.1757 | | 13.1887 | |
| | Hub | 17.5143 | | 16.5092 | |
| Deviation | Tip | 2.3473 | | 3.1269 | |
| | Mean | 2.7435 | | 3.3792 | |
| | Hub | 3.6146 | | 3.7198 | |
| Stagger | Tip | 62.3192 | | 10.2935 | |
| | Mean | 54.3443 | | 13.2152 | |
| | Hub | 40.0402 | | 18.0941 | |
| Vector Mean Angle | Tip | 63.7097 | | 11.9142 | |
| | Mean | 56.0706 | | 15.0171 | |
| | Hub | 42.6099 | | 20.2153 | |
| Vector Mean Velocity | Tip | 361.0539 | | 162.6028 | |
| | Mean | 286.5035 | | 164.7256 | |
| | Hub | 217.2856 | | 169.5438 | |
| Chord Radius | Tip | 0.2897 | | 0.1719 | |
| | Mean | 0.2086 | | 0.1437 | |
| | Hub | 0.1215 | | 0.1149 | |
| CL- Lift Coeff | Tip | 0.3229 | | 0.3757 | |
| | Mean | 0.3005 | | 0.3731 | |
| | Hub | 0.3102 | | 0.3662 | |
| CDp- Profile Drag Coeff | Tip | 0.0180 | | 0.0180 | |
| | Mean | 0.0180 | | 0.0180 | |
| | Hub | 0.0180 | | 0.0180 | |

Figure 5.3. Stage calculations at ACMC of initial design point, Part-3

| | | | |
|---|------|---------------|---------------|
| CDs- Secondary Drag Coeff | Tip | 0.0019 | 0.0025 |
| | Mean | 0.0016 | 0.0025 |
| | Hub | 0.0017 | 0.0024 |
| CDa- Endwall Drag Coeff | Tip | 0.0062 | 0.0098 |
| | Mean | 0.0048 | 0.0077 |
| | Hub | 0.0035 | 0.0057 |
| CD- TOTAL Drag Coeff | Tip | 0.0260 | 0.0304 |
| | Mean | 0.0245 | 0.0283 |
| | Hub | 0.0233 | 0.0261 |
| ω Total Loss Factor | Tip | 0.0706 | 0.0225 |
| | Mean | 0.0600 | 0.0264 |
| | Hub | 0.0534 | 0.0330 |
| Theoretical Pressure Rise | Tip | 0.2948 | 0.0563 |
| | Mean | 0.3177 | 0.0873 |
| | Hub | 0.3549 | 0.1503 |
| Entropy Delta | Tip | 11.8273 | 0.9854 |
| | Mean | 7.5438 | 1.2065 |
| | Hub | 4.5486 | 1.6518 |
| Entalpy Delta | Tip | 15348.9723 | |
| | Mean | 15348.9723 | |
| | Hub | 15348.9723 | |
| Cascade Efficiency | Tip | 0.7606 | 0.5999 |
| | Mean | 0.8112 | 0.6974 |
| | Hub | 0.8495 | 0.7804 |
| ω- Shock Loss Factor | Tip | 0.0107 | 0.0000 |
| | Mean | 0.0041 | 0.0000 |
| | Hub | 0.0000 | 0.0000 |

Figure 5.4. Stage calculations at ACMC of initial design point, Part-4

| POSTPROCESS | | Sta 1 | Sta 2 | Sta 3 | Sta 4 |
|---------------------|------|---------|--------|---------|--------|
| DF-Diffusion Factor | Tip | 0.1940 | | 0.1483 | |
| | Mean | 0.2209 | | 0.1620 | |
| | Hub | 0.2649 | | 0.1905 | |
| DF_equivalen- t DF | Tip | 1.3776 | | 1.2645 | |
| | Mean | 1.4073 | | 1.2815 | |
| | Hub | 1.4640 | | 1.3187 | |
| De Haller | Tip | 0.8531 | | 0.9464 | |
| | Mean | 0.8392 | | 0.9307 | |
| | Hub | 0.8160 | | 0.8980 | |
| Work Coeff | Tip | 0.1211 | 0.1356 | | |
| | Mean | 0.2127 | 0.2196 | | |
| | Hub | 0.4674 | 0.4152 | | |
| Flow Coeff | Tip | 0.4456 | 0.4790 | | |
| | Mean | 0.5906 | 0.6097 | | |
| | Hub | 0.8755 | 0.8383 | | |
| Camber Angle | Tip | 7.3225 | | 11.0183 | |
| | Mean | 10.1757 | | 13.1887 | |
| | Hub | 17.5143 | | 16.5092 | |
| Deviation Angle | Tip | 2.3473 | | 3.1269 | |
| | Mean | 2.7435 | | 3.3792 | |
| | Hub | 3.6146 | | 3.7198 | |
| σ -Solidity | Tip | 1.2058 | | 0.7503 | |
| | Mean | 1.5346 | | 0.9520 | |
| | Hub | 2.1101 | | 1.3022 | |
| s/c-Relative Pitch | Tip | 0.8293 | | 1.3328 | |
| | Mean | 0.6516 | | 1.0504 | |
| | Hub | 0.4739 | | 0.7679 | |
| h/c-Aspect Ratio | Tip | 2.6905 | | 2.7121 | |
| | Mean | 2.6905 | | 2.7121 | |
| | Hub | 2.6905 | | 2.7121 | |
| Absolute Mach | Tip | 0.4769 | 0.4916 | 0.4916 | 0.4640 |
| | Mean | 0.4769 | 0.5033 | 0.5033 | 0.4668 |
| | Hub | 0.4769 | 0.5298 | 0.5298 | 0.4732 |
| Relative Mach | Tip | 1.1715 | 0.9758 | | |
| | Mean | 0.9377 | 0.7691 | | |
| | Hub | 0.7239 | 0.5788 | | |

Figure 5.5. Post-processing parameters of APMC of initial design point

Table 5.1. Performance parameters of initial design point

| | |
|------------------------------------|--------|
| Mass Flow (Kg/Sec) | 20 |
| Compression Ratio | 1.1631 |
| Cascade Efficiency (Rotor) | 0.8112 |
| Cascade Efficiency (Stator) | 0.6974 |
| Cascade Efficiency (Stage) | 0.7987 |
| Speed (RPM) | 15300 |
| Inlet Total Pressure (Pa) | 101325 |
| Inlet Total Temperature (K) | 288 |

Input variables have been selected as annulus dimensions, mean line Alpha of Station 4, mean line Beta of Station 2. Radii of stations 2 and 3 are made equal to each other, thus 10 inputs were reduced to 8. The calculated number of design points is 81, with selecting the “enhanced template” option in ANSYS Workbench, the number of design points were increased to 161. Output variables were selected as compression ratio (CPR), stage efficiency, Diffusion Factor and De Haller number belongs to each blade and vane sections. Table 5.2 values were introduced to the Ansys Workbench optimization module.

Table 5.2. Input parameters, upper and lower limits for optimization

| Parameter Name | Symbol | Units | Lower Limit | Upper Limit |
|-------------------------|-------------------|--------------|--------------------|--------------------|
| Tip Radius of Station-1 | $r_{1,tip}$ | m | 0.22422 | 0.22422 |
| Tip Radius of Station-2 | $r_{2,tip}$ | m | 0.22620 | 0.21820 |
| Tip Radius of Station-3 | $r_{3,tip}$ | m | 0.22620 | 0.21820 |
| Tip Radius of Station-4 | $r_{4,tip}$ | m | 0.22620 | 0.21820 |
| Hub Radius of Station-1 | $r_{1,hub}$ | m | 0.11092 | 0.11092 |
| Hub Radius of Station-2 | $r_{2,hub}$ | m | 0.11305 | 0.12105 |
| Hub Radius of Station-3 | $r_{3,hub}$ | m | 0.11305 | 0.12105 |
| Hub Radius of Station-4 | $r_{4,hub}$ | m | 0.12500 | 0.11700 |
| Alpha Mean Station-4 | $\alpha_{4,mean}$ | ° | 12.00000 | 8.00000 |
| Beta Mean Station-2 | $\beta_{2,mean}$ | ° | 55.00000 | 48.00000 |

After performing multi-objective genetic algorithm optimization in Ansys Workbench utilizing face-centered central composite design (FCCCD) for DOE and response surface

method, candidate design points are calculated from 161 design points. The optimized results are given in Table 5.3

Table 5.3. Comparing input and output parameters before and after optimization

| | | | | Before Optimization | After Optimization | Difference % |
|-------------------------|---------------------------------|--------------------|-----------|---------------------|--------------------|--------------|
| Parameter Name | | Symbol | Units | 1 | 2 | 2-1 |
| Input Parameters | Tip Radius of Station-1 | $r_{1,tip}$ | m | 0.22220 | 0.22422 | 0.90164 |
| | Tip Radius of Station-2 | $r_{2,tip}$ | m | 0.21000 | 0.21858 | 3.92496 |
| | Tip Radius of Station-3 | $r_{3,tip}$ | m | 0.21000 | 0.21858 | 3.92496 |
| | Tip Radius of Station-4 | $r_{4,tip}$ | m | 0.21000 | 0.22292 | 5.79501 |
| | Hub Radius of Station-1 | $r_{1,hub}$ | m | 0.11310 | 0.11092 | -1.96402 |
| | Hub Radius of Station-2 | $r_{2,hub}$ | m | 0.12000 | 0.12041 | 0.33898 |
| | Hub Radius of Station-3 | $r_{3,hub}$ | m | 0.12000 | 0.12041 | 0.33898 |
| | Hub Radius of Station-4 | $r_{4,hub}$ | m | 0.12100 | 0.12037 | -0.52159 |
| | Alpha Mean Station-4 | $\alpha_{4,mean}$ | ° | 10.00000 | 10.29100 | 2.82771 |
| | Beta Mean Station-2 | $\beta_{2,mean}$ | ° | 52.00000 | 50.79500 | -2.37228 |
| Output Parameters | Compression Ratio | CPR | - | 1.16310 | 1.28740 | 9.65512 |
| | Stage Efficiency | η_s | - | 0.79870 | 0.85660 | 6.75928 |
| | Rotor Diffusion Factor At Tip | $DF_{rotor,tip}$ | - | 0.19402 | 0.26155 | 25.81847 |
| | Rotor Diffusion Factor At Mean | $DF_{rotor,mean}$ | - | 0.22094 | 0.33624 | 34.29140 |
| | Rotor Diffusion Factor At Hub | $DF_{rotor,hub}$ | - | 0.26490 | 0.43685 | 39.36143 |
| | Stator Diffusion Factor At Tip | $DF_{stator,tip}$ | - | 0.14828 | 0.38656 | 61.64069 |
| | Stator Diffusion Factor At Mean | $DF_{stator,mean}$ | - | 0.16201 | 0.41435 | 60.89893 |
| | Stator Diffusion Factor At Hub | $DF_{stator,hub}$ | - | 0.19051 | 0.46616 | 59.13172 |
| | Rotor DEHALLER At Tip | $DH_{rotor,tip}$ | - | 0.85314 | 0.81446 | -4.74934 |
| | Rotor DEHALLER At Mean | $DH_{rotor,mean}$ | - | 0.83921 | 0.76170 | -10.17681 |
| | Rotor DEHALLER At Hub | $DH_{rotor,hub}$ | - | 0.81596 | 0.69701 | -17.06678 |
| | Stator DEHALLER At Tip | $DH_{stator,tip}$ | - | 0.94639 | 0.82871 | -14.20092 |
| | Stator DEHALLER At Mean | $DH_{stator,mean}$ | - | 0.93069 | 0.78840 | -18.04798 |
| | Stator DEHALLER At Hub | $DH_{stator,hub}$ | - | 0.89802 | 0.71312 | -25.92823 |
| Centrifugal Root Stress | σ_{root} | MPa | 385.95000 | 400.62950 | 3.66411 | |

Candidate design points are the points, which are estimated from polynomials (Interpolated) thus they should be calculated again via the ACMC tool to validate if the output parameters match with input parameters. Recalculated parameters are given in the column called "After Optimization" in Table 5.3. A comparison chart for the variation in parameters that are stored in columns was given in Figure 5.6.

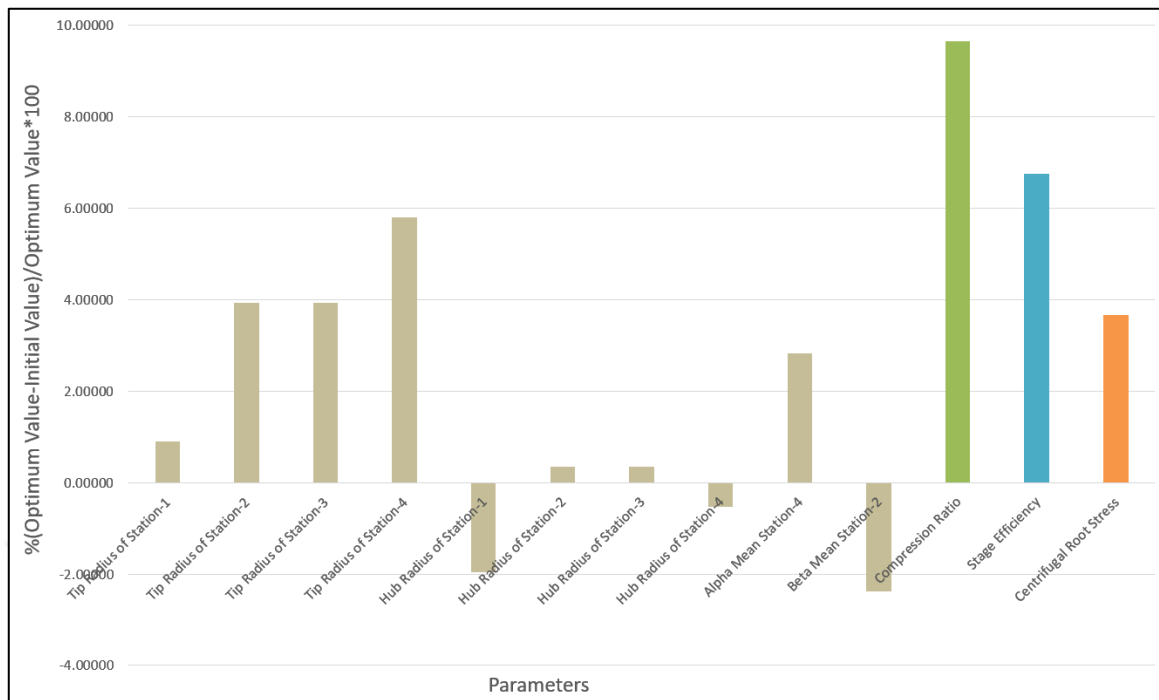


Figure 5.6. The variation between parameters of initial and optimum design points

In Figure 5.6, it is seen that a 9.65 percent improvement was attained in the compression ratio and 6.75 percent improvement in stage efficiency. On the other hand, a 3.66 percent increase in centrifugal stress has been encountered.

Stress calculations were conducted by utilizing equation 3.85. Validation of stress analysis was performed via Ansys Workbench. The model was prepared with a blade and an attached platform to the root section of the blade in order to read more realistic stress values. Figure 5.7 illustrates the FEA model.

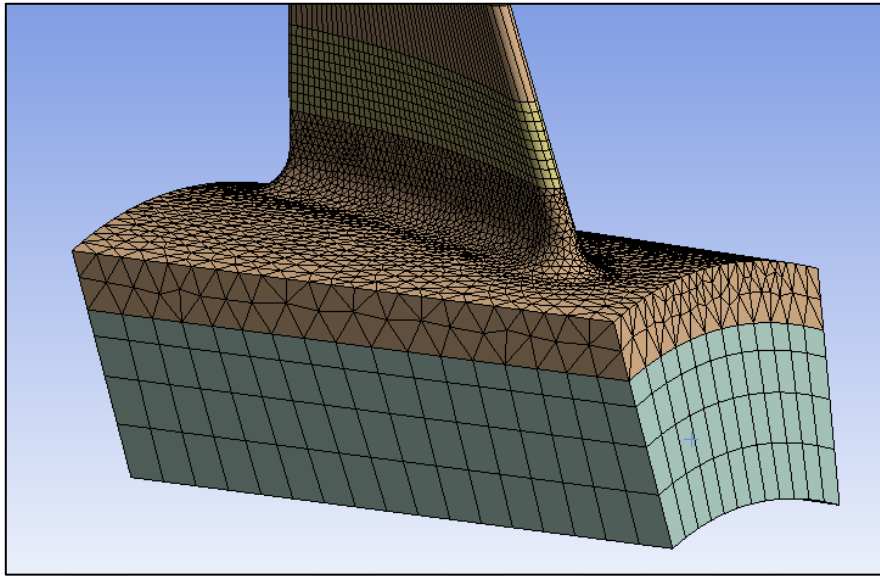


Figure 5.7. FEA model of the blade with root attachment

Blade aerofoil sections and solid models were constituted via NX. In order to reduce the internal stresses and the tilt stress, the sections are stacked as keeping coincidence about their area centers belong to each section individually. Parametric NX blade model is illustrated in Figure 5.8

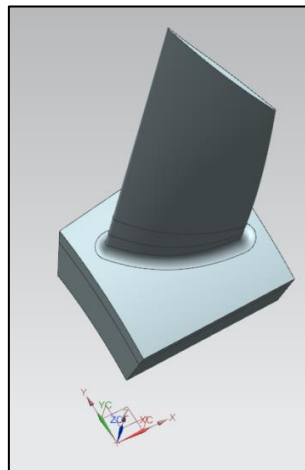


Figure 5.8. Parametric NX blade model

Types of the elements, which are used in the model, are SOLID186 and SOLID187. The number of elements is 33619 and the associated number of nodes is 65941. Only 15300 rpm was given to the model for initial condition and the model was fixed from the bottom surface of the platform via deformable remote point. FEA stress results are illustrated in Figure 5.9.

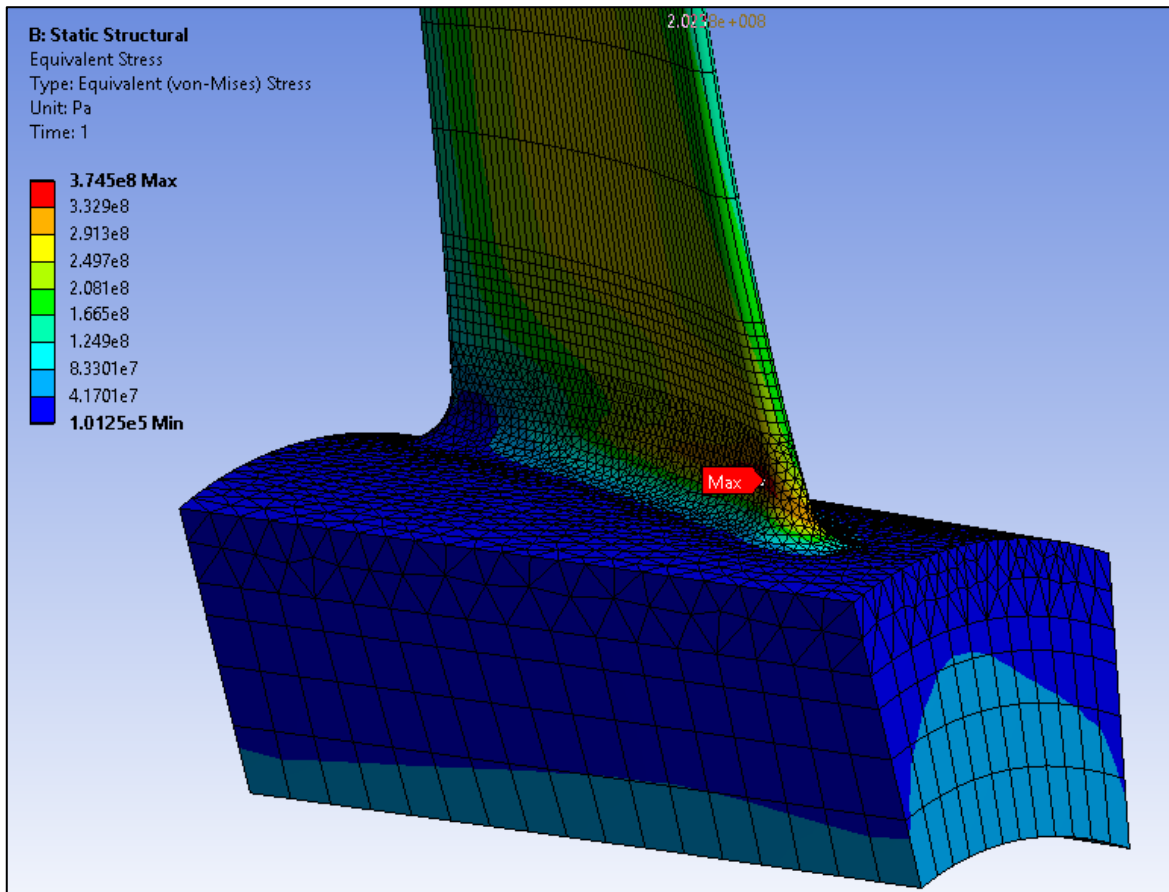


Figure 5.9. Von Mises Stress plot of the blade

The stress value was observed as 374MPa, which is very close to the analytic solution of 400MPa. If the blade material is selected as INCO 718, yield strength is given 980MPa and corresponding to literature criteria [2] the centrifugal stress on blades should be below 70 percent of material yield strength for preliminary design purpose. Thus allowable yield strength is calculated by $70\% \cdot 980 = 686\text{MPa}$, as a result of blade stress is much below that value, the design is safe in terms of centrifugal stresses. Among 161 design points, the min stress was encountered as 357MPa and max stress was encountered as 414MPa. It is seen

that the optimization process kept the stress in the allowable range while keeping the efficiency and compression ratio as maximum.

Modal analysis was conducted in order to assess if there exists a possible frequency match. The pre-stressed model was used so as to get a more realistic value of frequency at design speed. For preliminary design purposes, the first flexural mode frequency was investigated and read as 569 Hz from Ansys Workbench. The operating speed of the compressor is 15300rpm=255Hz. As a result of the calculated blade frequency of 569 Hz is much bigger than operating speed, therefore the design is safe in terms of resonance for the preliminary design concept. Advanced design stages entail checking all possible exciters. Campbell diagram should be prepared to avoid any coincidence of 1X, 2X, 3X,..., etc. engine order frequency and flexural, torsional and stripe mode frequency.

The compression ratio has been encountered as 1.1037 and 1.5198, min. and max. Values respectively among 161 design points. The selected optimized design point has a 1.2871 compression ratio and it is very close to the maximum value in the range. Stage efficiency has been encountered as 0.41 and 0.89, min and max values respectively. Selected optimized design point 5 has 0.8566 which is very close to the maximum value.

After completing optimization, analytical and CFD solutions were compared in order to assess 3D flow effects.

CFD grid creation was performed in Autogrid with considering following criteria: Maximum orthogonality and skewness > 15 , maximum expansion ratio < 5 , maximum aspect ratio < 4000 , maximum span wise angular deviation < 40 . The number of grids in rotor 1019655, number of grids in stator 592735, totally 1612390 grids were used. Spanwise number of mesh was determined as 65

Grid structure belongs to both rotor and stator passages are illustrated in Figure 5.10. Mean "y+" on blade walls are about 0.3 while the first cell thickness was given 1e-6m to all walls and the related plot is illustrated in Figure 5.11. The governing equations are the Reynolds Averaged Navier-Stokes equations (RANS); the turbulence model was selected as Spalart-Allmaras because of having good CFD agreement with the test result [26].

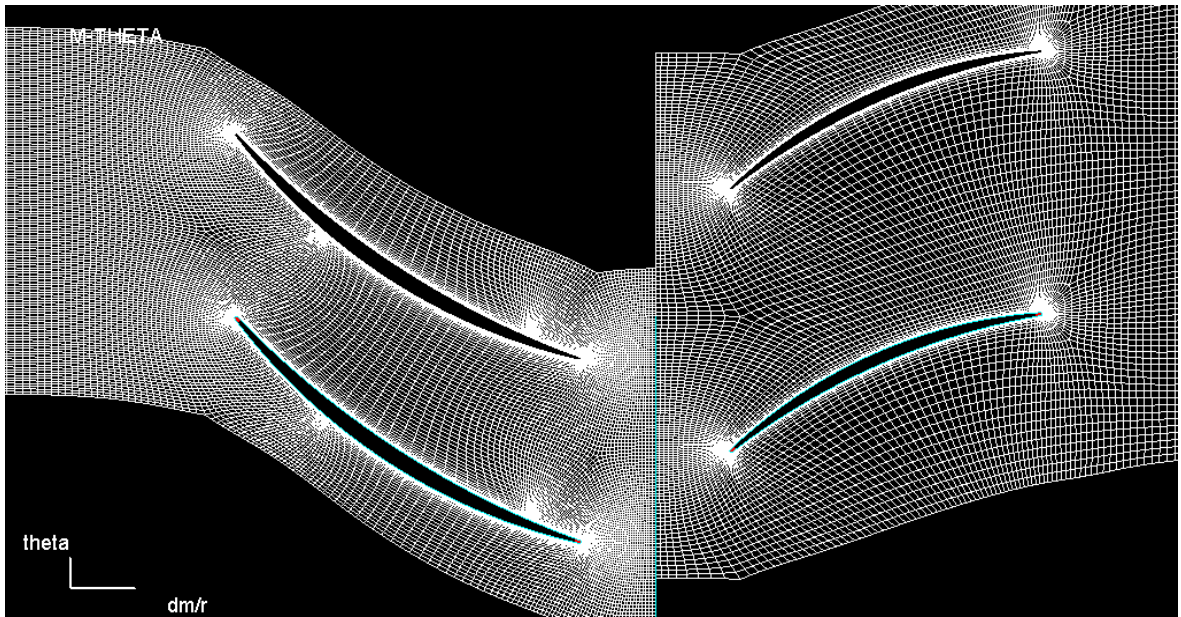


Figure 5.10. Grid structure for rotor and stator passages

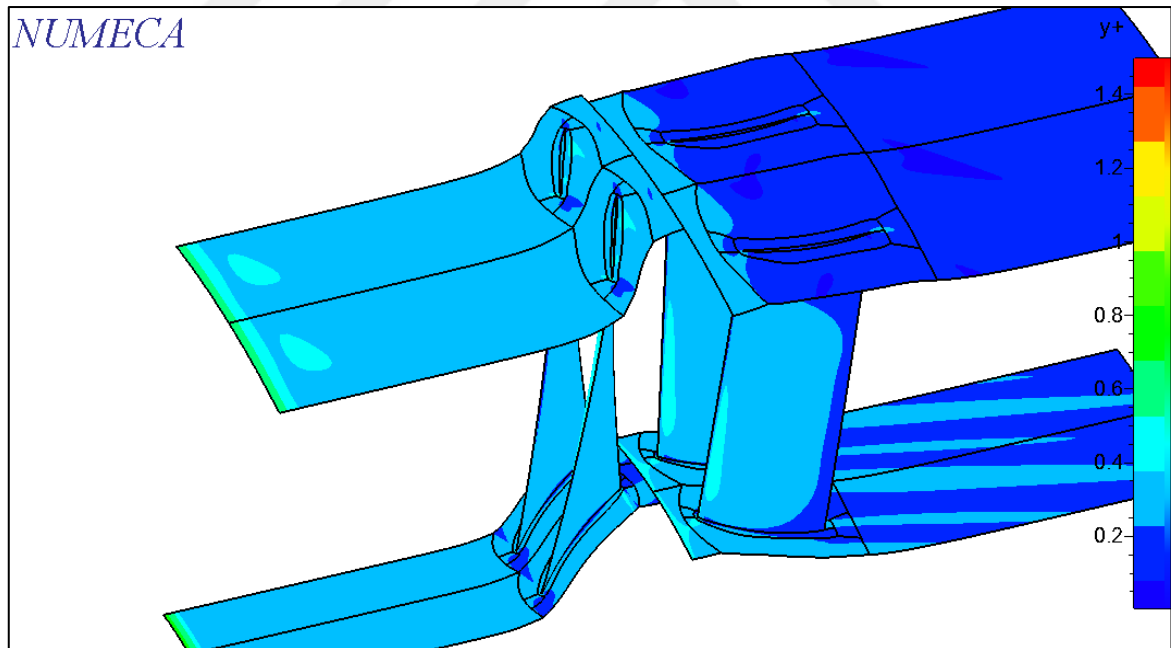


Figure 5.11. Y+ plot at surfaces

Table 5.4. The variation between CFD and analytical solution

| - | Mass Flowrate (kg/s) | Compression Ratio | Stage Efficiency |
|--|----------------------|-------------------|------------------|
| CFD | 19.52 | 1.285 | 0.8381 |
| Analytical Solution of Design Point 5 | 20 | 1.2874 | 0.8566 |
| % Difference | 2.459 | 0.1864 | 2.1597 |

CFD and analytical solutions were compared and the results are given by Table 5.4. The difference, which is encountered between CFD and analytical solutions of the mass flow rate is 2,459 percent. One of the basic reasons behind that difference is the sudden expansion region that occurs between Station 3 and Station 4. The flow separation region reduces the flow area this effect causes the blockage to be generated, which was mentioned earlier in section 3.2.5. Generated blockage region is illustrated in Figure 5.12 and 5.13.

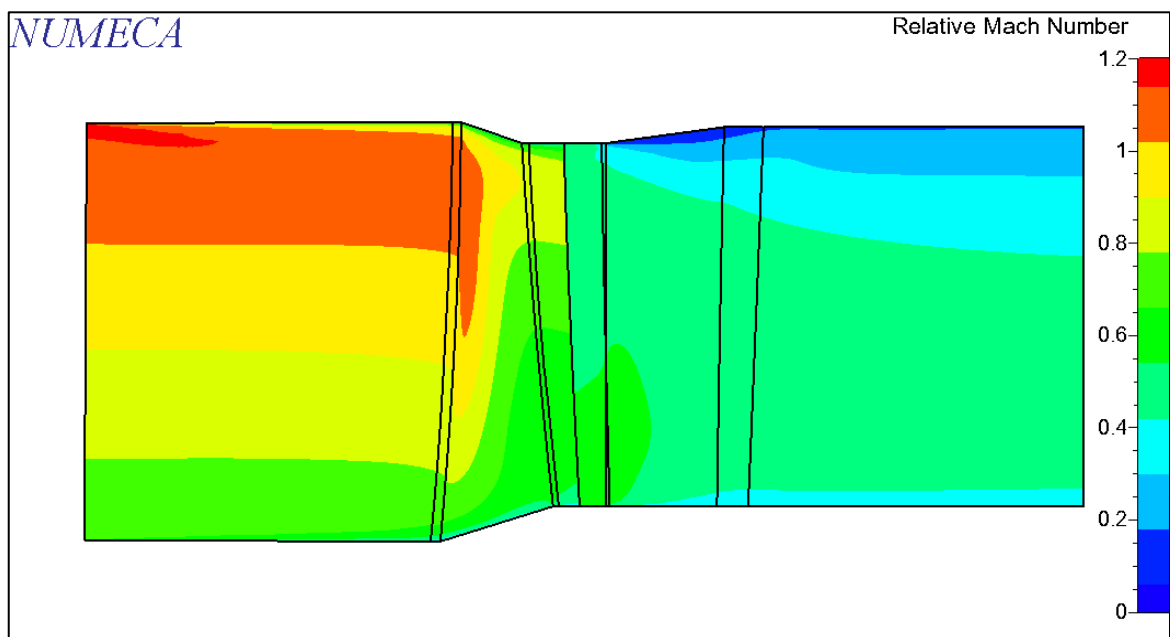


Figure 5.12. Meridional view of blockage region between Station-3 and Station-4

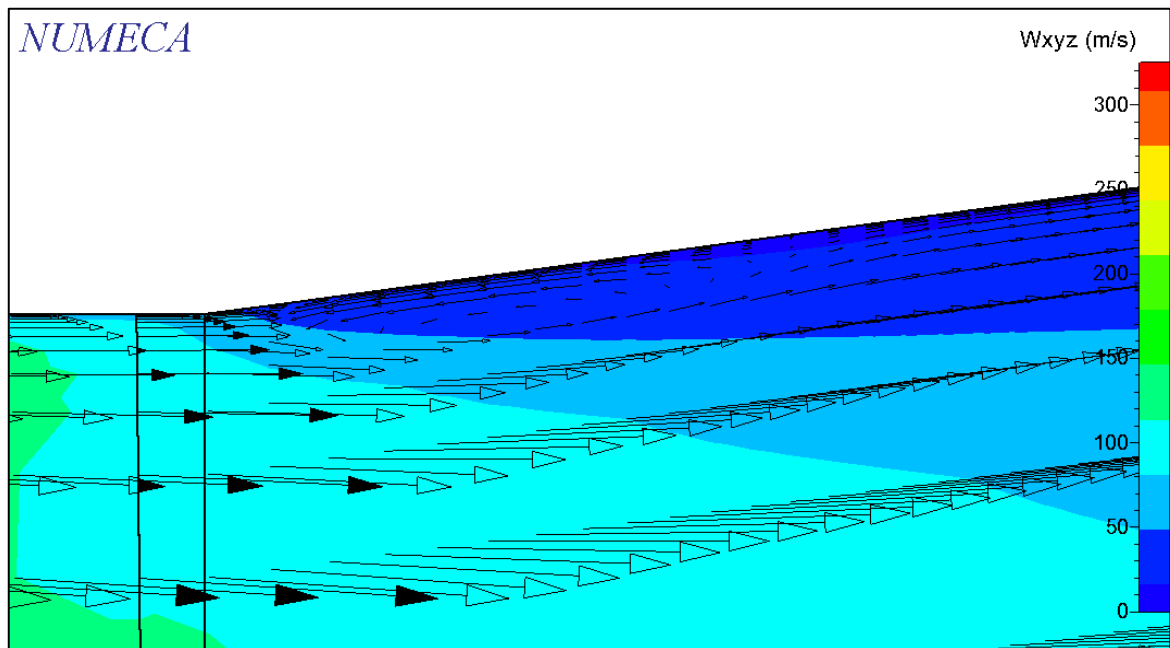


Figure 5.13. Closer view to blockage region between Station-3 and Station-4

If sudden expansion is prevented by the definition of optimization objectives by introducing a simple rule about the downstream sizes always be smaller than upstream sizes; therefore, the annulus is getting narrower through downstream. Blockage generation could be prevented and the effect of blockage is reduced. On the other hand, the transonic region is encountered as illustrated in Figure 5.14 and Figure 5.15 at the blade tip region where the relative Mach Number is around 1.2 which is very close to the analytical solution value of 1.1692. As we know that from Section 3.2.11 incoming relative velocity will increase while traveling over the suction surface and shock will occur in case of using highly curved profiles. The value of relative Mach Number when further proceeded over the suction surface is still about 1.2 and decrease steadily, because of using DCA blading. Instead of using DCA blading at the tip region, utilizing supersonic aerofoil contours would reduce the difference that is encountered between calculated values of mass flow rate, and the CFD results.

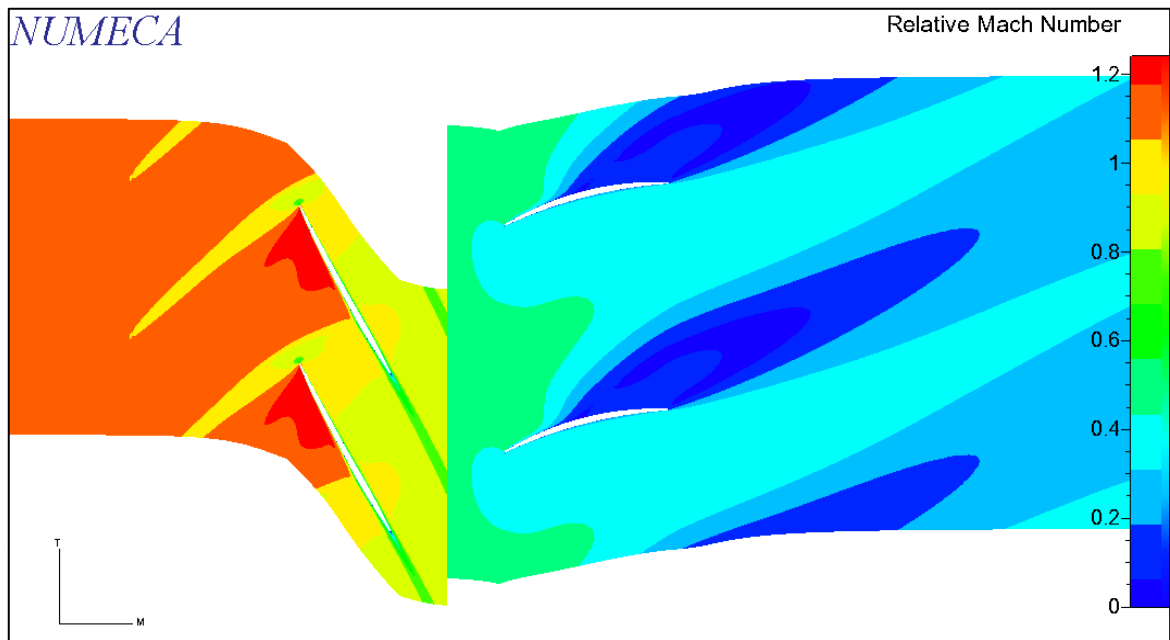


Figure 5.14. Blade to blade view, Relative Mach Number plot at 90% span

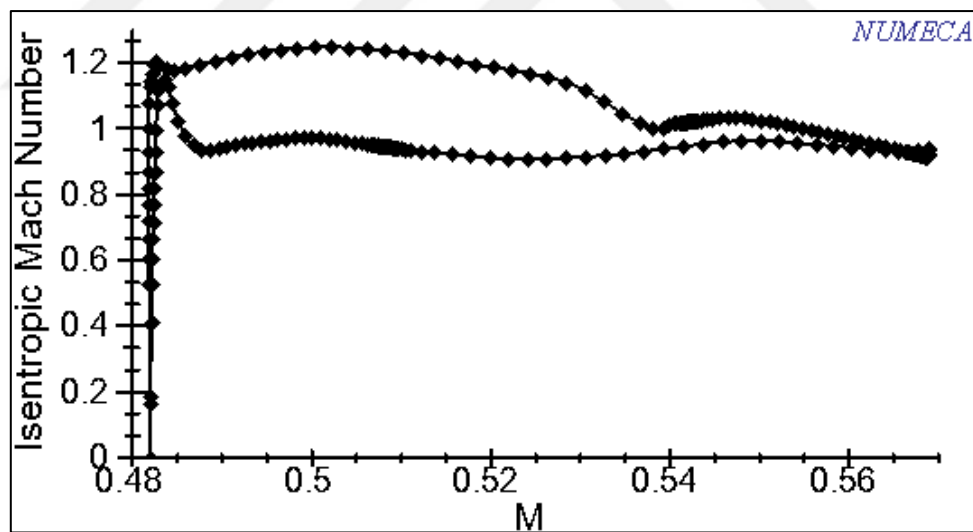


Figure 5.15. Isentropic Mach Number plot around blade at 90% span

At the blade span of 50 percent (Mean line), Blade to blade relative Mach Number figure is illustrated in Figure 5.16 and isentropic Mach number distribution plot around aerofoil is illustrated in Figure 5.17. Relative Mach Number is 1.6 around LE of the blade because of negative incidence, then it reduces to 0.8 through the downstream flow. This causes choking

in blade passage In case of introducing a "0" incidence angle would reduce relative Mach number to the calculated value of 0.9244.

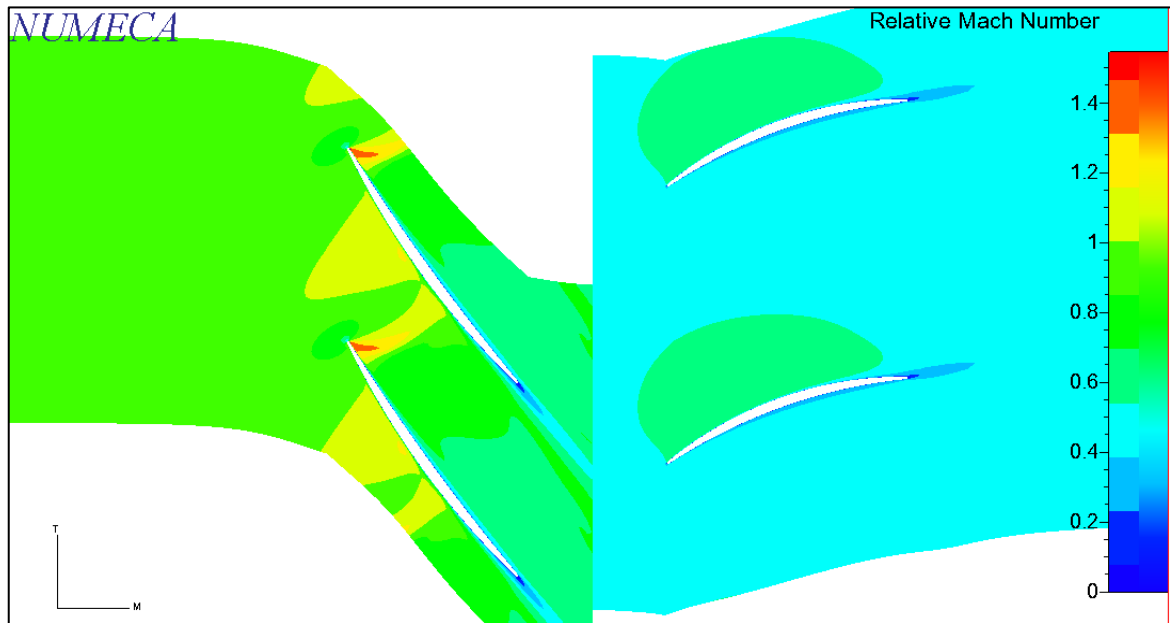


Figure 5.16. Blade to blade view, Relative Mach Number plot at 50% span

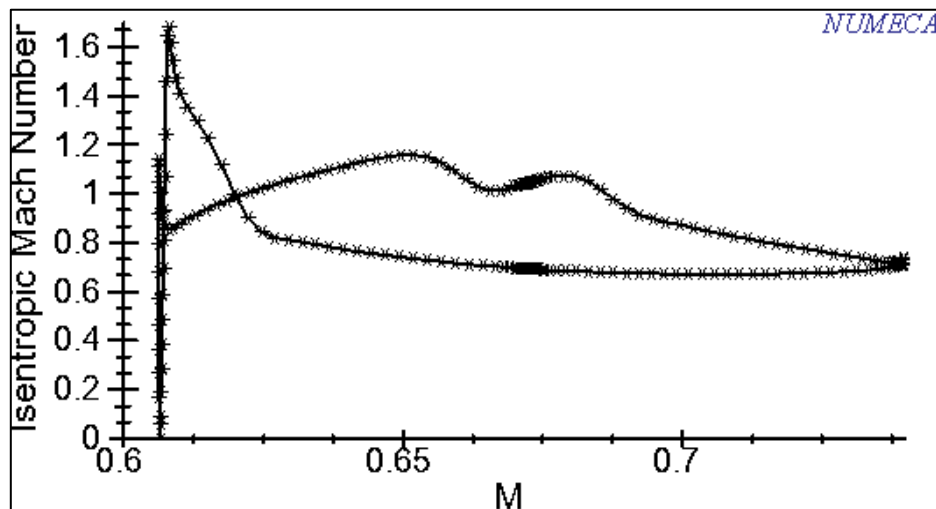


Figure 5.17. Isentropic Mach Number plot around blade at 50% span

At the blade span of 10 percent, Blade to blade relative Mach Number plot is illustrated in Figure 5.18. Relative Mach Number is 0.8 around LE of the blade, which is close to calculate the value of 0.7, then it reduces to 0.6 through the downstream flow.

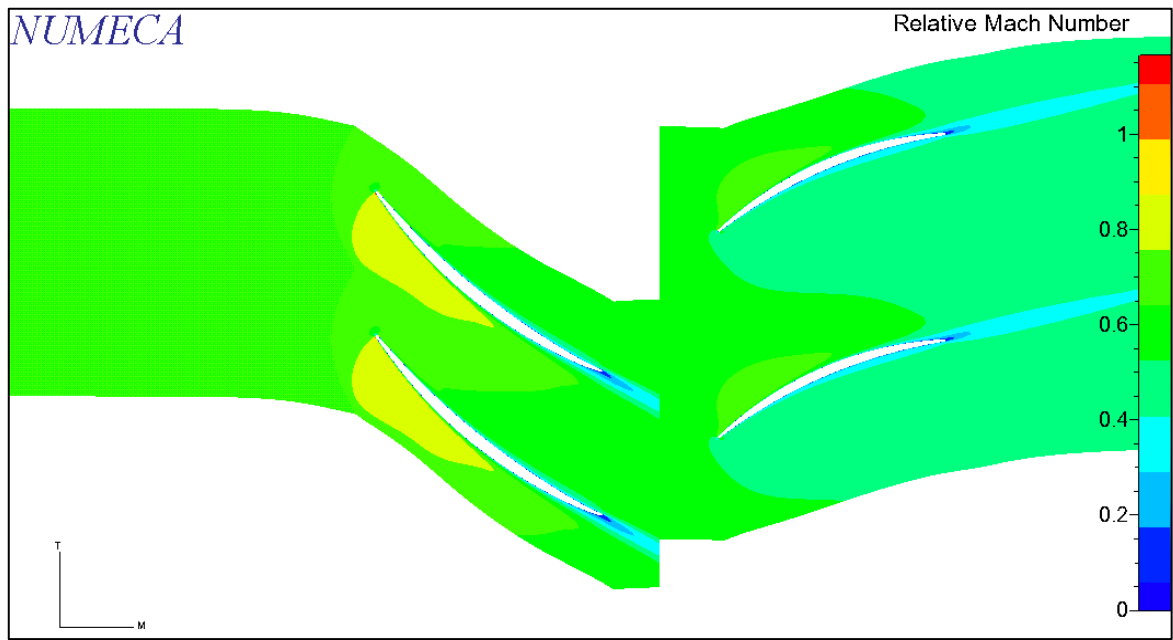


Figure 5.18. Blade to blade view, Relative Mach Number plot at 10% span

6. CONCLUSION

As it has been previously explained, mean line analysis is conducted in the preliminary design phase. Following aerodynamic calculations, steps are basically conducted through flow analysis, blade to blade analysis and CFD respectively. According to the comparison of APMC and CFD results, APMC provides a good estimation to the final CFD results in the meantime maintaining lower blade root stresses, highest efficiency, and highest compression ratio within a given annulus size limits and air angle ranges. Using the FEA method in optimization instead of analytical calculations might bring more realistic results by incorporating blade root geometric stress concentration and blade twist stress. For future improvements, off-design performance calculations might be incorporated as well. Supersonic blading at tip region would be a good option for the parametric NX blade generator. It would be a significant improvement in terms of reducing shock losses.

REFERENCES

1. Falck N. Axial flow compressor mean line design [dissertation]. Lund, Sweden: Lund University; 2008.
2. Saravanamuttoo HHH, Rogers GFC, Cohen H. *Gas turbine theory*. New York: Pearson Prentice Hall; 2009.
3. Pickavance D. European fighter aircraft engine design - intake, lp compressor and nozzle [dissertation]. London, England: Cranfield Institute of Technology; 1985.
4. Dener C. European fighter aircraft engine design - hp compressor and turbine [dissertation]. London, England: Cranfield Institute of Technology; 1985.
5. Oktay Ö. A preliminary design system for axial flow compressors [dissertation]. Ankara, Turkey: METU; 1996.
6. Mehel YS. Jet engine axial compressor design [dissertation]. Kocaeli, Turkey: Gebze Technical University; 2017.
7. Srikanth G, Prasad SS, Kumar VM, Reddy BM. Design methodology of a two stage axial compressor. *International Journal of Current Engineering and Technology*. 2014;(2):602-604.
8. Miller AS. Compressor conceptual design optimization [dissertation]. Atlanta, USA: Georgia Institute of Technology; 2015.
9. Chen GT, Greitzer EM, Tan CS MF. Similarity analysis of compressor tip clearance flow structure. *ASME Journal of Turbomachinery*. 1991;113(2):260-269.
10. Epstein A. Quantitative density visualization in a transonic compressor rotor. *ASME Journal of Engineering Power*. 1977;99(3):460-475.
11. Freeman C, Cumpsty N. Method for the prediction of supersonic compressor blade performance. *Journal of Propulsion Power*. 1992;8(1):199-203.
12. König W, Hennecke D, Fottner L. Improved blade profile loss and deviation angle models for advanced transonic compressor bladings: part II-a model for supersonic

- flow. *ASME Journal of Turbomachinery*. 1996;118(1):73-80.
13. Miller G, Jr. Lewis G, Hartmann M. Shock losses in transonic compressor blade rows. *ASME Journal of Engineering Power*. 1961;83(3):235-241.
 14. Wennerstrom A, Puterbaugh S. A three-dimensional model for the prediction of shock losses in compressor blade rows. *ASME Journal of Engineering for Gas Turbines Power*. 1984;106(2):295-299.
 15. Zhihui L, Yanming L. Optimization of rough transonic axial compressor. *Aerospace Science and Technology*. 2018;78(2):12-25.
 16. Dahlquist AN. Investigation of losses prediction methods in 1d for axial gas turbines [dissertation]. Lund, Sweden: Lund University; 1990.
 17. Dixon SL, Hall CA. Axial-flow compressors and ducted fans. *Fluid Mechanics and Thermodynamics of Turbomachinery*. 2010: 1-27.
 18. Lieblein S. Experimental flow in two dimensional cascades. *Aerodynamic design of axial compressors, NASA-SP-36*;1965:183-226.
 19. Cumpsty NA. *Compressor aerodynamics*. Essex: Longman Scientific & Technical; 2004.
 20. Hirsch C, Denton JD. Through flow calculations in axial turbomachines;1976 May 21; Köln: *Advisory Group for Aerospace Research & Development (AGARD)*; 1976.
 21. William HR, Robert JJ, Lieblein S. Blade element flow in annular cascades. *Aerodynamic design of axial compressors, NASA-SP-36*;1965:227-252.
 22. Koch CC, Smith LH. Loss sources and magnitudes in axial flow compressors. *ASME Journal of Engineering for Power*. 1976;98(3):411-424.
 23. Li Z, Zheng X. Review of design optimization methods for turbomachinery aerodynamics. *Progress in Aerospace Sciences*. 2017;93(1):1-23.
 24. Ağdacı O. Statistical investigation of mistuning behavior of bladed disc systems with ansys program [dissertation]. İstanbul, Turkey: ITU; 2017.
 25. Kor O. Aerodynamic optimization of a transonic aero-engine fan module

[dissertation]. İzmir, Turkey: İzmir Institute of Technology; 2016.

26. Gourdain N, Montagnac M, Boussuge JF. Numerical simulation of an axial compressor with non axisymmetric casing treatment. *European Conference for Aerospace Sciences, Progress in Propulsion Physics on*; 2009:EUCASS.

